

University of Alberta Library

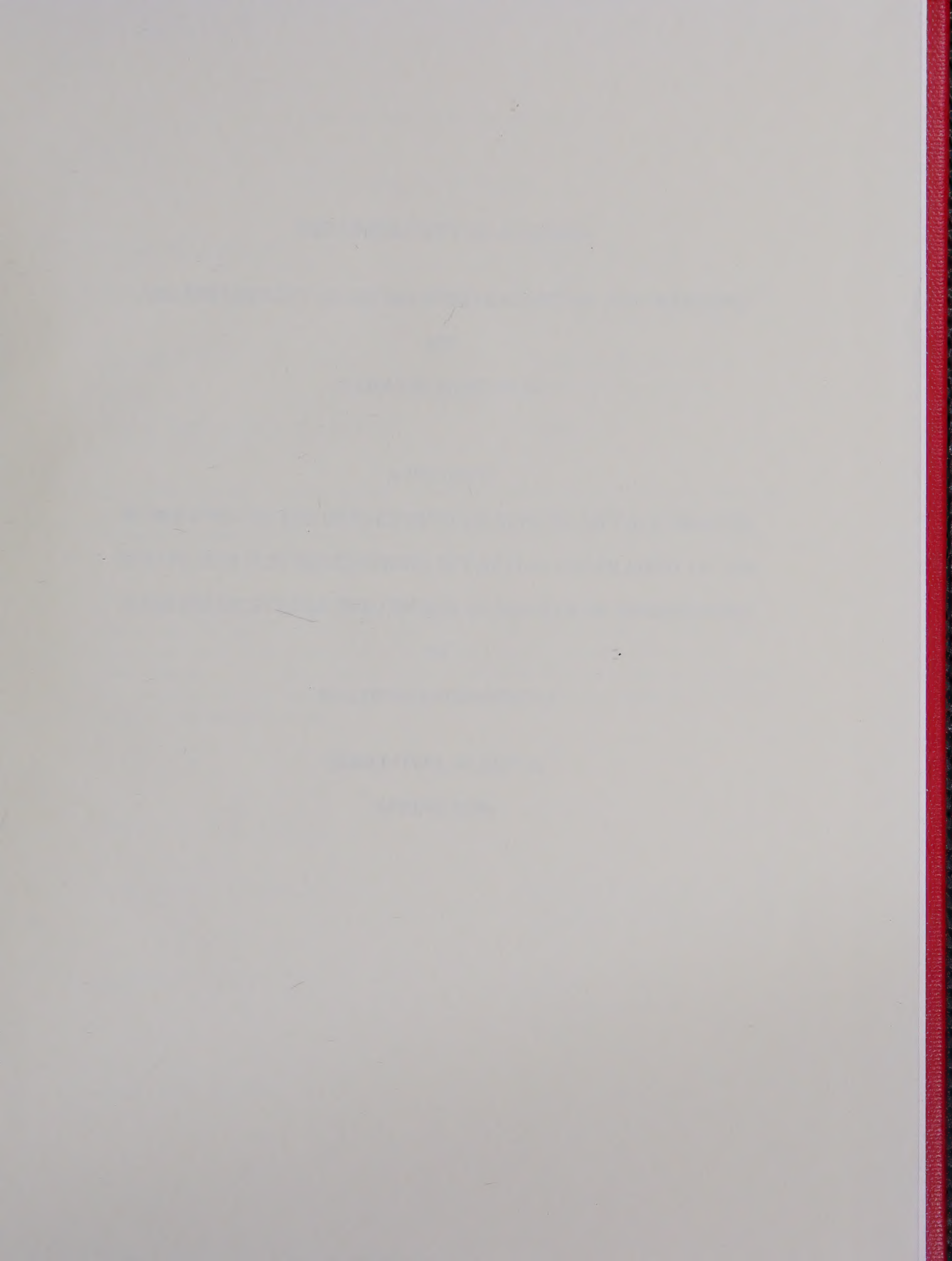


0 1620 3644044 2



Dept of Mining, Metallurgical  
and Petroleum Engineering  
University of Alberta  
Edmonton, Alberta  
Canada T6G 2G6







THE UNIVERSITY OF ALBERTA

RELEASE FORM

THE UNIVERSITY OF ALBERTA

NAME OF AUTHOR

THE ARC INSTABILITY IN MECHANIZED GAS METAL ARC WELDING

BY

TARAS D. SEMENIUK

YEAR THIS DEGREE WAS GRANTED

A PROJECT

SUBMITTED TO THE DEPARTMENT OF MINING, METALLURGICAL  
AND PETROLEUM ENGINEERING IN PARTIAL FULFILMENT OF THE  
REQUIREMENTS FOR THE DEGREE OF MASTER OF ENGINEERING

IN

WELDING ENGINEERING

EDMONTON, ALBERTA

SPRING 1996



Digitized by the Internet Archive  
in 2021 with funding from  
University of Alberta Libraries

<https://archive.org/details/Semeniuk1996>

THE UNIVERSITY OF ALBERTA

**RELEASE FORM**

NAME OF AUTHOR

Taras D. Semeniuk

TITLE OF PROJECT

Arc Instability in Mechanized  
Gas Metal Arc Welding

DEGREE

Master of Engineering in  
Welding Engineering

YEAR THIS DEGREE GRANTED

Spring 1996

Consistent with the terms of the Research Agreement dated September 28, 1995, the author releases this project to THE UNIVERSITY OF ALBERTA, NOVA GAS TRANSMISSION LTD., and LINCOLN ELECTRIC COMPANY OF CANADA LTD.

After the terms of the Research Agreement have been consummated, permission is granted to THE UNIVERSITY OF ALBERTA to reproduce single copies of this project and lend or sell such copies for private, scholarly or scientific research purposes only. The author reserves other publication rights, and neither the project nor extensive extracts from it may be printed or otherwise reproduced without the author's written permission.



UNIVERSITY OF ALBERTA  
FACULTY OF GRADUATE STUDIES AND RESEARCH

The undersigned certifies having read, and recommends to the Faculty of Graduate Studies and Research for acceptance, a project entitled ARC INSTABILITY IN MECHANIZED GAS METAL ARC WELDING submitted by TARAS D. SEMENIUK in partial fulfilment of the requirements for the degree MASTER OF ENGINEERING in WELDING ENGINEERING.



## **ABSTRACT**

Baseline performance of a Lincoln Electric PowerWave 450 Inverter power supply was successfully established. Bead-on-plate welds emulating Nova's hot pass parameters were made on ASTM A36 and IPSCO GR483 base metals. Acquired data was statistically and spectrally analyzed from which high information content parameters specific to arc instability phenomena in GMAW-S were established. The Inverter results were further compared to the performance of a conventional transformer-rectifier power supply under the same welding conditions. On A36, the power supplies performed comparably, while on GR483 the conventional power supply performed slightly better than the Inverter supply. Successful identification of GMAW-S process stability using spectral analysis methods is believed to be a first time achievement.



## **ACKNOWLEDGEMENTS**

The writer acknowledges the contributions of a few key individuals; Dr. Barry Patchett for technical guidance and expertise, Clark Bicknell for data acquisition and general experimental ingenuity; Dr. Pranob Banerjee for digital signal processing; and Christine Ouellet for reviewing report drafts.

This research work was made possible with the assistance of three companies; Nova Gas Transmission Ltd. for funding and supply of electrode wire; Lincoln Electric Company of Canada for temporary loan of the PowerWave 450 power supply; and IPSCO Inc. for the line pipe materials.



## TABLE OF CONTENTS

	PAGE
1.0 INTRODUCTION .....	1
2.0 LITERATURE REVIEW .....	3
3.0 EXPERIMENTAL METHOD .....	26
4.0 RESULTS .....	33
5.0 DISCUSSION .....	42
6.0 CONCLUSIONS .....	53
7.0 RECOMMENDATIONS .....	54
8.0 TABLES .....	55
9.0 FIGURES .....	60
10.0 REFERENCES .....	85
11.0 APPENDICES .....	88



## LIST OF TABLES

	PAGE
Table 1: Base metal composition. ....	56
Table 2: Hot pass welding parameters. ....	57
Table 3: Wire feed speed calibration. ....	58
Table 4: Arc voltage calibration. ....	58
Table 5: Spectral analysis peak frequencies. ....	58
Table 6: Process characterization parameters for GMAW-S. ....	59
Table 7: Overall power supply performance. ....	59



## LIST OF FIGURES

	PAGE
Figure 1:	Metal transfer modes in arc welding. ....
Figure 2:	Instantaneous arc voltage and current variation during short-circuiting transfer. ....
Figure 3:	Schematic representation of stable and unstable arcs. ....
Figure 4:	Arc pressure as a function of droplet dimensions. ....
Figure 5:	Mode 1 weld pool oscillation. ....
Figure 6:	Base metal and strongback assembly. ....
Figure 7:	Static resistance arc voltage calibration. ....
Figure 8:	Data acquisition virtual image block diagram. ....
Figure 9:	Data acquisition set-up. ....
Figure 10:	Spatter spark trails. ....
Figure 11:	Completed welds. ....
Figure 12:	Electrode tips. ....
Figure 13:	Key to oscillogram signatures. ....
Figure 14:	4 second oscillograms. ....
Figure 15:	1 second oscillograms. ....
Figure 16:	0.2 second oscillograms. ....
Figure 17:	Short circuit frequency. ....
Figure 18:	Short circuit duration. ....
Figure 19:	Instantaneous short circuit ratio. ....



Figure 20:	Arc duration .....	78
Figure 21:	Arc coefficient of variation. ....	79
Figure 22:	Histogram of short circuit frequency. ....	80
Figure 23:	Histogram of short circuit duration. ....	81
Figure 24:	Histogram of arc duration. ....	82
Figure 25:	Spectral analysis of GMAW-S (FFT). ....	83
Figure 26:	Comparison of time and frequency domain SCF. ....	84



## LIST OF APPENDICES

	PAGE
Appendix A: Chemical Composition of Thyssen K-Nova Wire. ....	89
Appendix B: Matlab & Unix Commands for Spectral Analysis. ....	92
Appendix C: FFT Frequency Conversion. ....	97
Appendix D: Initial Spatter Spark Trail Photographs . ....	99
Appendix E: Parametric Spectral Analysis of Linde SVI on A36. ....	102
Appendix F: Research Agreement. ....	104



## LIST OF SYMBOLS, INITIALISMS & ACRONYMS

AGA	American Gas Association
AI	Artificial Intelligence
Ca	Calcium
DCEP	Direct Current Electrode Positive
FCAW	Flux Cored Arc Welding
$f_D$	Droplet transfer rate
FFT	Fast Fourier Transform
GMAW	Gas Metal Arc Welding
GMAW-P	Pulsed transfer GMAW
GMAW-S	Short-circuit transfer GMAW
GTAW	Gas Tungsten Arc Welding
NGTL	Nova Gas Transmission Ltd.
ppm	Parts per million (wt%*10000)
REM	Rare Earth Metals
SCF	Short Circuit Frequency
SCR	Silicon Controlled Rectifier
SMAW	Shielded Metal Arc Welding
STT	Surface Tension Transfer
$t_D$	Droplet transfer time
$t_{SC}$	Short circuit duration
WIC	Welding Institute of Canada
WPOF	Weld Pool Oscillation Frequency



## **1.0 INTRODUCTION**

Mechanized Gas Metal Arc Welding utilizing short-circuit metal transfer (GMAW-S) is the preferred method for field welding of large-diameter pipelines. The short-circuiting, or dip transfer, mode of metal transfer provides all-position capabilities with minimal sensitivity to pipe residual magnetism while simultaneously minimizing levels of ultraviolet radiation produced.

In some steel making practices, calcium (Ca) is added to modern pipeline steels to minimize sulfur levels and modify inclusion morphology. Unfortunately, Ca based oxysulfide inclusions may detrimentally affect the stability of the welding arc causing plasma flaring which may induce flaws in the weld-bead, e.g. step-like defects and lack of fusion. Spatter generation is also increased with high levels of the calcium-oxysulfide inclusions.

Nova Gas Transmission Ltd. (NGTL) has found that the first external weld pass, or hot pass, is most susceptible to arc stability effects.

The original purpose of this research was to attempt to control arc stability in GMAW-S using a programmable power supply. The Lincoln Electric PowerWave 450 power supply and associated waveform software were to be used for process control. It was thought this action would over-ride calcium inclusion induced flaring, and thus promote a more regular short circuit metal transfer event. Unfortunately, contract complications did not allow release of the required software in time to be used for the present research.



Consistent with the original experiment purpose, a baseline comparison of two GMAW power supplies welding on two types of base metal was performed. Experimental directives were then modified to further examine statistical and spectral differences in the baseline responses.



## 2.0 LITERATURE REVIEW

Prior to welding experiments, a review of available literature was performed on: metal transfer, arc stability, flaw formation, weld pool oscillation effects, power supplies, statistical parameters, and the Fast Fourier Transform method of spectral analysis. Findings are summarized in the following sub-sections.

### 2.1 GMAW-S Metal Transfer

Liu and Siewert<sup>1</sup> provide a reasonable account of metal transfer in GMAW. The modes of metal transfer in arc welding are schematically illustrated by Figure 1. At relatively low-current and low-voltage levels short circuit transfer (intermittent-bridging transfer) occurs.

Figure 2 schematically shows one complete metal transfer cycle of GMAW-S. In the short circuiting mode, the electrode feed rate is slightly higher than the melting rate, so that the tip of the electrode eventually dips into the molten pool and extinguishes the arc. During the short circuit, the voltage drops to near-zero and the current rises very rapidly. The high current causes resistance heating of the electrode which subsequently begins to melt. The electromagnetic pinch force (Lorentz force) aids in detaching the molten droplet from the electrode tip. Surface tension also plays an important role in the necking of the electrode tip while gravity plays a lesser role. Finally, the neck breaks and the droplet is transferred. At this point, the arc is re-ignited and the voltage reaches its peak value while the current begins to decrease. The tip of the electrode continues to melt as it moves toward the



molten pool. This entire process repeats at approximately 20 to 200 cycles per second (Hz).

## 2.2 Arc Stability

Arc spatial stability refers to the relative stability of the arc in space. Instability arises as the arc moves to follow mobile cathode spots located on the surface of the weld pool. In contrast to spatial stability, electrical stability is concerned with how difficult it is to strike and maintain the arc.<sup>2</sup> Both spatial and electrical stability are important in overall process stability and concomitant weld quality.

### 2.2.1 Work Function

One of the ways in which electrons are produced at the cathode spot is by field emission. This type of emission is generally used to explain welding arcs involving non-thermionic cathodes.<sup>2</sup>

In field emission, the work function of electron emitting sites is fundamentally important to both arc and electrical stability. Field emission of electrons occurs in metals that boil at temperatures below that required for thermionic emission of electrons, e.g. most engineering metals.<sup>3</sup> A simplified definition of work function is the energy required to remove an electron from a material, and thus, represents a barrier to spontaneous decomposition of matter. The intensity of the energy barrier is described by units of electron-volts (eV).<sup>4</sup>



Lesnewich<sup>4</sup> through his references explained emission from oxides in the welding arc. It was thought that concentration of current at small oxide sites causes the emitting oxides to be heated by their own resistance. Oxide heating further reduces the work function permitting even more electrons to be supplied for heating (and emission). The cascading cycle continues until the oxide is heated beyond its decomposition temperature and is destroyed. Work function was also explained as being dependent on the magnitude of the electric field outside the emitter surface, and the orientation of the surface to the underlying crystal lattice. Values for relevant oxides were given as:

<u>Work Function (eV)</u>	
CaO at 930 °F (500 °C)	2.37
Al <sub>2</sub> O <sub>3</sub> at 2050 °F (1120 °C)	4.7

In contrast to the oxide work function values reported by Lesnewich, Michaelson<sup>5</sup> summarized elemental values:

<u>Work Function (eV)</u>	
Calcium (Ca)	2.87
Cerium (Ce)	2.9
Iron (Fe)	4.5
Aluminum (Al)	4.28

The above elemental values represent solid state photoelectric measurements. Specimen purity, measurement method, and distribution of crystallographic facets account for a 0.1-0.2 eV margin of variability. No data were provided for elevated



temperature or liquid state conditions. Sulfur, oxygen and oxides were not included in Michaelson's summary.

Lancaster<sup>3,6</sup> explained that two types of non-thermionic cathode emissions are probable with a gas shielded welding process: tunneling and switching. In the case of thin films such as aluminum (<10 nm), a high electric field forms if positive ions condense on the oxide surface. When the field is higher than about  $10^9$  V/m, electrons may tunnel through the film and generate an emitting site. Alternatively, the electric field may cause the oxide to be locally conductive.

For thicker films, or films with dielectric properties that do not allow the build up of the required field, e.g. copper or iron, a phenomenon known as switching makes the film locally conductive. Similar to tunneling, switching also requires the surface to become charged by positive ions.

For both types of cathode emission, the individual emitting sites are in the order of 100 nm in diameter and have lifetimes ranging from 1 ns to 1 ms. The effect of emission is to detach oxide from the metal surface and generate small but intense jets of metal vapor and debris.

### 2.2.2 Arc Physics

It is known that field emission occurs in GMAW-S with DCRP. Electrons are literally ripped out of the weld pool (cathode) by the concentrated arc voltage electric field near the cathode surface. Electron emission is concentrated at small, mobile cathode “spots.” The mobility of these emission sites causes arc spatial



instability since the arc wanders to follow the path of least resistance. With simple C-Mn steels, the sheer number of emission sites present in the weld pool tends to produce a relatively stable net emission despite their random motion.<sup>2</sup>

When elements or compounds are introduced in the weld pool that have a greatly reduced work function, electron emission becomes concentrated at these sites. Research work at the University of Alberta has suggested the concentrated emission results in formation of “reverse plasma jets” due to the concentration of most of the arc current on one cathode spot.<sup>7</sup> Arc spatial instability with calcium treated and also REM steels has been attributed to the formation of these reverse jets.

Through conversations with B.M. Patchett and A.C. Bicknell, it is theorized that a reversal in arc pressure occurs when the relative size of the anode and cathode arc roots are reversed. The driving force for arc pressure are Lorentz compressive forces acting on the welding arc. The magnitudes of the electromagnetic Lorentz forces are a function of current density and are independent of polarity. When the concentrated electron emission from low work function sites occurs, the current density at the constricted arc root markedly increases. Figure 3 schematically shows the reverse plasma jet formation and its interaction with the “normal” jet. It is believed reverse plasma jets support the molten droplet at the electrode tip, and thus cause extended arc flaring during GMAW-S. The occurrence of arc flaring is manifested by a decrease in short circuit frequency (SCF) and an increase in weld spatter.<sup>7,8</sup>



According to Lancaster, there may be four possible sources of cathode and anode jets:<sup>6</sup>

- (1) Bulk disintegration of electrode material in which the jet contains relatively large pieces of non-molten electrode. Explosion of gas inside the electrode causes electrode fragmentation in materials such as cadmium, zinc, brass and copper.
- (2) Vaporization of surface layers of metal oxide and other impurities at the cathode and anode spots. Charged particle interaction with the surfaces is required.
- (3) Chemical reaction generated gas, particularly oxidation of carbon and steel to produce CO and CO<sub>2</sub>.
- (4) Electromagnetically induced flow of gas in the arc column which is directed away from the constriction at the electrode.

(1), (2) and (3) originate at the electrode surface and are called anode or cathode jets. (4) is commonly termed “plasma jet.” All the above jets give rise to an apparent “stiffness” to parts of the arc near the electrodes.

In 1967, Naylor and Guile<sup>9</sup> suggested anode and cathode jets can sometimes collide and influence the arc. Their experimentation showed that brass electrode vapor was carried into the arc by “high speed jets,” i.e., Lancaster’s source (1). Anode and cathode jet collision were clearly shown with an actual photograph by Milner and Apps.<sup>10</sup> The anode, and likely the cathode material, were copper in this case, i.e.,



also Lancaster's source (1). The collision of anode and cathode jets was apparently discussed by Finkelnburg and Maecker back in 1956.

Excluding anode, cathode or plasma jet collisions, literature presents a few other possibilities for molten droplet suspension/repulsion in GMAW. These are:

- (i) the reaction force from small intense metal vapor jets<sup>6</sup>
- (ii) chemical reaction and vaporization of oxides<sup>6</sup>
- (iii) restraining plasma jet<sup>11</sup>
- (iv) a Lorentz force exerted on the plasma<sup>12</sup>
- (v) electron pressure<sup>2,13</sup>

Point (i) corresponds to source (1) of the anode or cathode jet description provided by Lancaster<sup>6</sup> and is not relevant for ferrous materials. Point (ii) appears to combine (2) and (3) and may play a role in pendant droplet behavior. Continuous vaporization or gas evolution to suspend/repel the molten droplet is not considered likely, therefore, point (ii) is thought to play an intermittent role (*Semeniuk opinion*).

Point (iii) depicts 1963 observations by Smith.<sup>11</sup> Cooksey and Milner<sup>13</sup> (1966) produced experimental evidence that did not support the plasma jet explanation. These authors further questioned whether the observed repulsive behavior was in fact repulsion. It was suggested anode spot movement on the weld pool simply creates turbulence within the molten droplet and provides the observed disturbed motion.

Point (iv) is similar to Greene's original theory of emission area control of metal transfer. Using DCEP and argon shielding on mild steel, Waszink and Gratt<sup>12</sup>



provided theoretical and experimental evidence of an upward pressure on the pendant droplet. At low current ( $< 100$  A), a small diameter anode spot exists on the electrode tip. However, since the anode spot is actually composed of two concentric annuli with the outer annulus having a higher electron density, a localized current divergence occurs within the droplet. It was argued that the higher current density of the anode spot causes Lorentz induced plasma compression immediately adjacent to the anode spot. This action tends to suspend the pendant droplet. Referring to Figure 4, calculations showed the upward force exists when  $\alpha < \beta$ . Note upward pressure was only present at a welding current less than 100 A in both the theoretical model and experimental evidence. This relatively low welding current is about half the value used in depositing the hot pass. A recognized shortcoming of Waszink and Gratt's research lies in the fact that vapor pressure and the force of fluid entering the droplet were not accounted for.

Point (v) describes another possibility for pendant drop suspension. Cooksey and Milner<sup>13</sup> indicated electron pressure is capable of suspending a droplet with DCEN. Patchett<sup>2</sup> explained electron pressure is only an emitter phenomenon (cathode) and does not play a role in suspending the molten droplet during electron capture (anode). The high current density in the vicinity of the cathode spot provides the "electron pressure" necessary to suspend the droplet. In this explanation, droplet suspension is not related to electron movement, i.e., kinetic energy.

Glickstein and Yeniscavisch<sup>14</sup> reported on the effect of calcium additions on arc physics. Using GTAW, calcium was shown to have a significantly greater reduction in anode fall space voltage than virtually all other minor elements.



It has also been suggested that with non-thermionic cathodes, electrons are emitted with a velocity parallel to the cathode surface. This may explain rapid random movement of individual emitting sites.<sup>6</sup>

### 2.2.3 Rare Earth Effects

Murthy and Loper<sup>15</sup> examined arc and metal transfer in steels containing rare earth metals (REM) using GMAW-S. Using oscillograms and high speed video, low work function electron emitters were shown to encourage the growth of large molten globules at the electrode tip. Metal transfer occurred by globular-bridging with the weld pool. Flaring and arc wandering was typical of an unstable condition. Li and Patchett<sup>8</sup> found similar results.

In DCEP welding, REM present in the weld pool reduces the cathode work function, promotes cathode-jet formation and tends to confine the arc due to activation (reduction in work function).<sup>15</sup> Cathode jets can transfer more energy to the wire electrode (anode) and increase its melting rate at a given wire feed rate. This results in an increase in arc length (voltage) and a decrease in welding current. The decrease in current further encourages growth of large globules due to a sharp drop in electromagnetic pinch force. Ratz *et al.*<sup>16</sup> referred to work by Ludwig (1968) where additions of about 0.08% Ca or about 0.03% REM in HSLA steels reduced arc potential and hence the pinch force. The relationship between calcium and pinch force as explained by Ludwig may not be entirely correct since calcium likely affects arc voltage independent of arc length (*B.M. Patchett, U. of A.*).



#### 2.2.4 Calcium Treated Steels

In steel making, calcium is injected into the melt to combine with (remove) sulfur and hence improve toughness. Patchett and Bicknell<sup>7</sup> performed specific work on late 1980's IPSCO pipeline steels. The steels used in their experimentation had higher levels of calcium than present IPSCO steels, e.g. 60 ppm versus 50 ppm max. It was shown that certain low work function inclusions in the pipe material caused extended arc flaring and concomitant decrease in SCF. The identified problem inclusions were ranked in order of decreasing effect as: Ca, Ce, Ti, Nb, and Mn. A complex relationship was shown to exist from which an empirical regression equation depicting overall instability for microalloyed steels was developed:<sup>7</sup>

$$X = 0.169(CaS + CeS) + 0.27(Ca + Ce) + 0.018Ti + 0.025Cb - 0.015Al + 0.0025Mn - 0.0018Si \quad (1)$$

if  $S > Ca + Ce$ , then  $(CaS + CeS) = Ca + Ce$   
and  $(Ca + Ce) = 0$

if  $S < Ca + Ce$ , then  $(CaS + CeS) = S$   
 and  $(Ca + Ce) = Ca + Ce - S$

For pure CO<sub>2</sub> shielding:

$X < 20$	Negligible effects (SCF = 80 to 100)
$20 < X < 50$	Random minor instabilities (SCF = 40 to 80)
$50 < X < 63$	Random major instabilities (SCF = 30 to 40)



$63 < X < 70$  Constant major instabilities (SCF = 25 to 33)

$X > 70$  Constant severe instabilities (SCF = < 25)

Note, for Equation (1), values are in parts per million (ppm) and not in weight percent.

Inclusion size, number, and distribution were also found to be factors in arc stability. It was thought that the size of MnCaS inclusions played perhaps the greatest role in the intensity of arc flaring and reverse plasma jet formation.

Much of Patchett and Bicknell's investigation focused on gas optimization. It was shown that arc stability improved by decreasing the oxidizing potential of the shielding gas. It was further recommended the most practical approach to the arc stability problem would be with procedural development.

Villafuerte and Gedeon<sup>17</sup> recently completed their work on counteracting calcium induced arc instability during GMA welding using artificial intelligence power supplies. Comparisons were made between a conventional constant voltage power supply and an "artificially intelligent spatter free" supply. IPSCO GR483 steels having calcium levels ranging from 1 to 34 ppm were welded with Nova's current hot pass parameters. Calcium levels were found to have the most significant effect on spatter levels, arc flaring, SCF, and penetration. Spatter was significantly reduced by increasing inductance in the conventional power supply.

Previous work by the Welding Institute of Canada (WIC) had shown that calcium tends to increase the interval of arcing but does not affect the short-circuit duration. WIC also found that arc duration tended to be lower with a CRC-Evans groove



preparation than bead-on-plate runs for the same pipe material. Bead-on-plate runs were determined to provide acceptable results for identifying general trends in arc parameters and spatter quantification.

In general, the WIC approach to the arc stability problem was an attempt to quantify arc parameters with specific attention to the current rise rate,  $dI/dt$ , and the effect of inductance.

## 2.3 Flaw Formation

### 2.3.1 Spatter

Gupta and Gupta<sup>18</sup> provided a comprehensive review of spatter generation from a European and former Soviet Union perspective. Fundamentally, any phenomenon that causes the arc to be unstable results in spatter. The spatter can be caused by:

- severing of the molten bridge
- expulsion of residue metal from the electrode
- expulsion of large droplets by the force breaking the bridge
- weld pool oscillation
- expulsion of large droplets from the electrode
- abrupt evolution of CO<sub>2</sub> from the weld pool and/or electrode tip

It has been experimentally shown that the amount of spatter is related to the rate and nature of oxidation at the electrode tip. With CO<sub>2</sub> and Ar-O<sub>2</sub> shielding gases, spatter losses increased with the alloy content of the electrode wire. Inconsistency in



experimental results exists with respect to electrode carbon content and spatter generation.

For minimum spatter the most significant variable is arc length; it should be very short. As the external component of the arc length increases, such as with a wandering arc, spatter generation increases. Spatter has been shown to increase smoothly as the electrode was given either a forehand or backhand angle of inclination.

In short circuit mode, spatter is largely dependent upon the current when the molten bridge is broken. By reducing the short circuiting current, the amount of spatter can also be reduced. Power source design allowing a 0.1-1 ms current reduction of 2-10 A at the start of each short circuit promotes stability. The optimum level of induction, which controls the rate of current rise, has been shown to be 60 kA/s for wire diameters of 0.8, 1.2 and 1.6 mm. However, SCF and the ratio of short-circuit-duration to arc duration were also reduced, i.e., less metal transfer.

By reducing or eliminating the number of instantaneous short circuit events, the amount of spatter was shown to decrease. The optimum ratio of arc time to cycle duration was determined to be 0.6 to 0.8.

Patchett and Bicknell<sup>7</sup> reported, that with extended arc flaring, reverse plasma jets cause random ejection of electrode pendant droplets. This condition can be accentuated by weld pool oscillation. During forward slumping of the weld pool, the weld pool crater becomes more constricted and thus tends to increase the vertical deflection of the arc towards the droplet. The combined effect of the reverse plasma jet and deflected arc were considered to increase the amount of spatter.



To summarize, any arc event that causes spatial instability results in spatter generation. The amount of spatter in GMAW-S can be minimized but not eliminated.

### 2.3.2 Step-like Defects

Based on oscillograms and high speed cine films, Sasaki *et al.*<sup>19</sup> explained step-like defect origin. These “flaws” were thought to result from too much metal being deposited per transfer event due to an extremely extended period between short circuits. The advancing solidification front of the solid/liquid interface, located at the rear of the molten pool, then “freezes in” the excess volume of electrode material. Li and Patchett<sup>8</sup> explained that erratic metal transfer events tend to get “frozen in” with high travel speeds.

### 2.3.3 Lack of Fusion

Li and Patchett<sup>8</sup> further suggested that the preceding step-like defects produced with bead-on-plate welds can result in lack of fusion with groove welds.

Lancaster<sup>3</sup> showed through calculations that the occurrence of lack of fusion depends on the relative temperature of the molten metal and the solid interface. Thermal conductivity of both liquid and solid phases needs to be taken into account in order to assess the likelihood of lack of fusion. During the short circuit portion of the GMAW-S cycle, when the arc is extinguished, lack of fusion occurs when



molten metal comes in contact with non-molten metal and solidifies as a “cold shut.”

## 2.4 Weld Pool Oscillation Effects

G. den Ouden *et al.*<sup>20</sup> showed through experimentation that weld pool oscillation plays a significant role in overall process stability in GMAW-S. The process is most stable when the short circuit frequency (SCF) is equal to the weld pool oscillation frequency (WPOF).

Weld pool oscillations are triggered by the momentum of liquid metal being injected into the weld pool at the moment of liquid bridge rupture. In addition, the abrupt generation of arc pressure immediately following arc re-ignition also has oscillation effects. Mechanical disturbance of the work piece can also cause oscillation in some cases. The oscillations damp out rapidly due to viscosity and solidification effects (loss of energy).

Wire feed speed is also important in process stability. At low wire feed speed ( $SCF < WPOF$ ) the oscillating weld pool surface misses the growing droplet at the end of the electrode one or more times before contact is made. This results in a more random SCF, increased variability in droplet size, more spatter, etc. At higher wire feed speed ( $SCF > WPOF$ ) the arc length becomes so short that stubbing of the electrode in the weld pool predominates, also leading to irregularity and instability of the welding process.



In GMAW-S with a partial penetration weld (e.g. hot pass) a Mode 1 oscillation predominates. Mode 1 oscillation is a symmetric mode characterized by vertical movement of the liquid metal in the weld pool (Figure 4). Mathematically, Mode 1 oscillation can be described by the following equation:<sup>20</sup>

$$\text{WPOF}_p = 5.84 (\gamma / \rho_L)^{1/2} D_1^{-3/2} \quad (2)$$

where:

$\text{WPOF}_p$	=	partial penetration weld pool oscillation frequency.
$\gamma$	=	surface tension of liquid metal.
$\rho_L$	=	density of liquid metal.
$D_1$	=	equivalent diameter of the partially penetrated weld pool, i.e., diameter of the circle having an area equal to the surface area of the weld pool.

Experimentation with 85Ar-15CO<sub>2</sub> and pure CO<sub>2</sub> showed a linear relationship between Equation 2 and SCF, i.e., process optimization occurs when SCF = WPOF<sub>p</sub>.



## 2.5 Power Supplies

Three recently published papers on relevant state of the art power supplies were reviewed:

- Lincoln STT
- Panasonic AI Inverter
- Fronius T.I.M.E.

Some bias inherently existed in the papers as each was written by a representative of a specific power supply manufacturer.

Stava<sup>21</sup> reported on a relatively new power supply designed specifically for semi-automatic GMAW-S. Lincoln's surface-tension-transfer (STT) supply operates neither in the constant current nor constant voltage mode. The power to the arc is based on the instantaneous arc requirements, not on "average DC voltage." Electrode current can be adjusted in the order of microseconds.

Claimed benefits of this power supply were:

- substantially reduced spatter
- ease of welding (a feature that maintains arc stability for variations in extension length)
- lower arc radiation and fume generation
- reduced heat input on thin-gauge material



Real time sensing of arc voltage is the key parameter in the STT. Based on the instantaneous arc voltage, five separate microsecond current adjustments can be made depending on the stage in the short circuiting process. In addition, within the pinch mode a continuous calculation of the rate of change of the shorted voltage with respect to time is made ( $dV/dt$ ). When a pre-set  $dV/dt$  has been reached, indicating that fuse separation is about to occur, the current is reduced in microseconds to a low level, thus nullifying explosive arc re-ignition.

Improved welding operation was shown by somewhat limited experimentation. Photographs were taken during welding comparing the spatter spark trails of the STT and a conventional power supply (1 sec. exposure at  $f_{16}$ ). These photographs and photographs of completed welds clearly showed less spatter generation with the STT.

One limitation of the STT, as identified by WIC<sup>17</sup> in their arc stability experimentation, is insufficient current capacity for hot pass welding (Nova parameters).

Nacey<sup>22</sup> described Panasonic's fourth generation artificial intelligence (AI) inverter power supplies for GMAW-S. Reduced spatter generation, faster travel speeds and better arc striking capabilities were cited as benefits. Compared to conventional SCR power supplies, the AI supplies were identified as having faster response times, dynamic response capabilities, and more arc control variables.

Experiments showed that by manipulating peak current time, peak short circuit current during arc re-ignition, and average base current level, the weight of spatter generated could be minimized. Compared to a conventional SCR supply, the AI



supply showed reduced spatter generation over a wider range of arc voltage settings (with CO<sub>2</sub> shielding).

With AI supplies, the operator simply dials procedural variables such as: shielding gas type, wire diameter, and welding current. The AI computer microprocessor then selects the optimum internal dynamic variables: peak current level, base current level, re-ignition current, arcing period time, and short circuit time. The operator can fine tune the voltage setting and optimization of dynamic variables is simultaneously performed by the AI supply. Similar to the STT supply described by Stava,<sup>21</sup> feed-back circuitry exists to provide real time arc monitoring.

Although the specific model of Panasonic power supply used for the preceding experimentation was not identified, WIC<sup>17</sup> in their arc stability work compared the Panasonic RF350 inverter to a conventional power supply. WIC found that for high calcium IPSCO pipeline steel, no significant difference existed between the two power supplies with respect to spatter levels and welding arc parameters (short circuit duration, open arc duration, maximum current).

Lahnsteiner<sup>23</sup> described advances in synergic inverter GMAW power supplies from Fronius' (Austria) perspective. Synergic refers to "single knob" control providing an optimum combination of some 46 different GMAW-S variables. One of the highlighted improvements of this supply is a programmed pulse of current that occurs when the weld run is completed. The pulse ensures no droplet retention occurs at the electrode tip, and thus alleviates the need to snip the end of the electrode prior to commencing the next weld. To minimize spatter generation, short circuit current rise rate can also be adjusted based on the wire composition, diameter, and shielding gas type.



The Fronius T.I.M.E. power supply contains self tests to assist in fault finding. For example, subroutines are available to quickly check external cables, welding torch contacts, wire-feed roller slippage and linearity, feeder motor current, open circuit voltage, and perform a Hallshunt-test.

In addition, to meet ISO 9000 requirements, continuous documentation of welding parameters is inherent. The output can either be printed or connected to a central quality control work station in the case where multiple power supplies are in use.

No experimental support for the preceding claims was provided.

## 2.6 Statistical Parameters

By applying real time data acquisition of welding current and voltage, a great deal of information on process stability can be obtained. No definite agreement in which parameters are most important for statistical analysis was identified in the literature.

Lucas<sup>24</sup> used the standard deviation of the peak current measurements as the indicator of GMAW-S process stability and uniformity. For a particular current level, the voltage that provided the minimum standard deviation in peak current was correlated with the optimum welding potential, as determined during welding. Lucas also used histograms depicting the number of short circuit current peaks as a function of current setting to show stable and unstable welding conditions.



In research work for the American Gas Association (AGA), Li and Patchett<sup>8</sup> reported process stability in terms of SCF. A ratio comparing SCF values of RE steels and C-Mn steels was also shown to be useful for describing the effect of RE additions.

$$R = \frac{SCF_{RE}}{SCF_{C-Mn}} \quad (3)$$

The ratio of SCF at different welding speeds versus shielding gas composition and/or electrode polarity, for different electrode wires, was used to show the high sensitivity of SCF<sub>RE</sub> to procedural variables.

$$R = \frac{SCF_{1000\text{mm/min}}}{SCF_{200\text{ mm/min}}} \quad (4)$$

These researchers, and some of their references, also used weld penetration measurements to further describe process behavior.

In their experimental work on GMAW-S, Liu and Siewert<sup>1</sup> determined the time needed for successive droplet transfers ( $t_D$ ) in GMAW-S using instantaneous welding current and voltage data. The researchers suggested statistical analysis be performed on  $t_D$  to determine the mean, standard deviation, standard error, and maximum and minimum values. The preceding parameters were considered best for characterizing metal transfer. Welding parameters with the smallest variation in  $t_D$  were shown to also be those with the shortest transfer period, least spatter and smoothest bead surface.



Droplet transfer rate ( $f_D$ ) was also identified as providing information on process stability. Droplet transfer rate ( $f_D$ ) was defined as the inverse of the time period between two consecutive droplets ( $1/t_D$ ). Either the distribution of  $f_D$  or the distribution of  $t_D$  could be used to assess process stability.

Pokhodnya *et al.*<sup>25</sup> described statistical methods in the course of describing work at the EO Paton Welding Institute on Shielded Metal Arc Welding (SMAW-DC). The short circuit duration,  $t_{SC}$ , was identified as a “high information content parameter” used to describe metal transfer. By counting the number of events versus  $t_{SC}$  and displaying the results on a histogram, the delineation between random (instantaneous) short circuits and metal transfer short circuits was clearly shown. A threshold value of  $t_{SC}$  for true metal transfer could also be readily obtained from the histogram approach. In addition to  $t_{SC}$ , the variance in instantaneous values of the arc voltage,  $s^2$ , was also described as being an important statistical parameter.

The average and standard deviation of short circuit voltage, arc voltage, short circuit current, and welding arc current, were also described using histograms. The distribution of the number of events versus either voltage or current was shown. The area contained within the histogram describes the probability of a specific phenomenon. The ratio of respective areas was used to describe the degree of process stability, e.g. arc voltage + open circuit voltage versus short circuit voltage.

By manipulating weld procedure variables such that welding voltage, arc current standard deviation, and arc current coefficient of variance were minimized, arc stability was shown to improve.



## 2.7 Fast Fourier Transform (FFT)

Fourier analysis can be used to further process acquired data and provide process information. Signals are transformed from time domain to frequency domain using the FFT technique. The FFT is useful in providing information about hidden periodicities in the signals. For example, welding voltage usually contains multiple components: arc voltage, line voltage, voltage fluctuations (as result of metal transfer and weld pool oscillation), background noise, etc.<sup>26</sup> In some cases, the hidden periodicities of the frequency spectrum can be discerned and the results used for process analysis.

G. den Ouden *et al.*<sup>20</sup> used a FFT program to calculate the oscillation frequency of the molten weld pool. By first filtering out low frequency arc current pulses, the weld pool oscillation frequency was calculated with a reported accuracy of 1 Hz.

Wang *et al.*<sup>26</sup> used the FFT spectral analysis technique to characterize metal transfer in Flux Cored Arc Welding (FCAW). The results of their FFT analyses were used to generate a metal transfer mode map in which an operating window for smooth spray transfer was identified. They found the FFT spectra correlated well with the metal transfer mode and provided simpler and more conclusive results than a spatter collection and measurement approach. With spray or globular metal transfer, resolvable frequencies were clearly identified, even with mixed mode conditions. However, with short circuit FCAW, results were less conclusive as no characteristic frequency was identified. They attributed their *noisy* signal response to the relatively large voltage changes occurring in short circuit metal transfer (>10 V).



## **3.0 EXPERIMENTAL METHOD**

This section provides an account of the method used in the experimentation. Background information and explanations are provided where necessary.

### **3.1 Baseline Power Supply Performance**

The initial test matrix consisted of two power supplies and two base metals:

<u>Power Supplies</u>	<u>Base Metals</u>
Linde SVI-400	ASTM A36
Lincoln PowerWave 450	IPSCO GR483 (#426507)

As explained in the Introduction (Section 1.0), this matrix was not expanded to include PowerWave 450 waveform development.

#### **3.1.1 Power Supplies**

##### Linde SVI-400

The Linde SVI-400 is a three phase constant voltage, transformer-rectifier type DC power supply with continuously adjustable slope, voltage and inductance controls.

The rated output of the Linde SVI-400 is:

400 A, 40 V at 100% duty cycle.



## PowerWave 450

The Lincoln Electric PowerWave 450 is a digitally controlled inverter power source capable of high-speed waveform control.<sup>28</sup> It is designed to be used as a synergic welding system in conjunction with the Synergic 7 wire feeder.

Intrinsic welding processes are: GMAW, GMAW-S, GMAW-P, FCAW, and SMAW. With GMAW and FCAW, an operator prescribed change in wire feed speed automatically results in the supply optimizing the voltage. However, some degree of non-synergic control is maintained by the welding operator.

The rated output of the PowerWave 450 is:

500 A, 40 V at 60% duty cycle.

One external control on the PowerWave 450 is the “Wave Control.” This control provides a way of changing arc behaviour without creating a new welding procedure. In GMAW, wave control adjusts the inductance. Increasing the wave control setting decreases the inductance, which results in the arc getting colder and pinched tighter.

### **3.1.2 Base Metals**

Two steels were used for baseline power supply comparisons: ASTM A36 and IPSCO GR483 (Heat #426507). ASTM A36 is a material known to favour stable short circuit transfer. Previous research<sup>7</sup> showed IPSCO Heat #426507 material



promoted significant arc instability. Table 1 shows the chemical composition of the two base metals.

The chemical compositions of A36 and #426507 were used to predict the degree of arc instability using Equation 1 (Section 2.2.4).<sup>7</sup> The instability formula showed the SCF should decrease by at least 50% from 40-80 Hz for A36 to 25-33 Hz for #426507.

### **3.1.3 Specimen Preparation**

Plate and pipe specimens were torch cut from the respective materials and fillet welded to 75 X 100 X 430 mm strongbacks (Figure 6). The strongback was necessary to prevent distortion and thus maintain contact tube to work distance. Weld side surfaces were ground to remove mill scale and provide comparable finishes.

### **3.1.4 Equipment Calibration**

Travel speed was controlled by moving the workpiece with respect to a stationary arc. A variable speed lathe bed was set to provide an arc travel speed in accordance with Nova hot pass parameters (Table 2).

Actual wire feed rates were compared to front panel settings. Small discrepancies of approximately -3% and +1.8% were identified for the SVI and PowerWave



respectively (Table 3). Wire feed rate was subsequently set at  $\approx$ 12330 mm/min for both power supplies.

Oscillograms of weld set-up runs showed that variation in arc voltage existed between the two supplies (for a set voltage of 25 V). To enable meaningful performance comparisons, it became necessary to over-ride the front panel voltage values, and thus equalize the respective arc voltages. This procedure was accomplished with the aid of a water cooled static resistance box containing 11 feet of 1/4" diameter stainless steel tubing. Figure 7 schematically shows the arc voltage calibration set-up. Based on measured static resistance and the appearance of the completed welds, arc voltage was iteratively set at 24.3 V for both power supplies. Results of the arc voltage calibration are summarized in Table 4.

Consistent with PowerWave 450 Operator's Manual, manipulation of the Wave Control had no effect on the static arc voltage. Iterative welding runs on A36 indicated the optimum Wave Control setting was "high." On this setting the welding process was audibly more stable and weld profiles were less peaked than with either the "low" or "medium" settings.

### **3.1.5 Data Acquisition**

During welding runs, arc voltage and time data was acquired using LabVIEW 2.2 software. Figure 8 shows the virtual image block diagram for both acquisition and analysis. Four seconds of weld data were acquired at a sampling rate of 1000 Hz.



### **3.1.6 Welding Runs**

Bead-on-plate welds were made with the two power supplies on the two base metals. Welding parameters were in accordance with Nova's present hot pass procedures, with exception of shielding gas flow rate (Table 2). The CO<sub>2</sub> gas flow rate was reduced from 2.1 to 0.9 m<sup>3</sup>/hr given the absence of wind with "indoor" laboratory welding conditions.

Figure 9 schematically shows the experimental set-up. Data acquisition was commenced approximately 3-4 seconds after welding had started to allow ample time for process stabilization.

Photographs were taken during welding in an attempt to quantify the amount of spatter generated. A Canon AE1 SLR camera loaded with ASA 400 film and a 50 mm lens (1:1.8) was used. Arc to film distance was 1.7 m, lens aperture was f<sub>22</sub>, and exposure time was 1 second. Macro-photographs of completed welds and representative electrode wire stubs were also taken.

### **3.1.7 Statistical Analysis**

Acquired arc voltage and time data were examined with the aid of LabVIEW Version 2.0 statistical analysis and Microsoft Excel Version 5.0 Chart and Histogram functions. Specific parameters examined were:



- Short Circuit Frequency (SCF)
- Short Circuit Duration
- Instantaneous Short Circuit Ratio
- Arc Duration
- Arc Coefficient of Variation

Instantaneous Short Circuit Ratio describes the number of instantaneous short circuits with respect to total short circuits. To be classified as an instantaneous short circuit two criteria must be met; the short circuit duration must be less than 1 ms and the time between successive short circuits less than 5 ms. Instantaneous short circuits primarily result from weld pool oscillation effects, and do not represent true “dip transfer” (metal transfer event).

Arc Coefficient of Variation is a statistical parameter determined by dividing the arc duration standard deviation by the mean arc duration. This relative dispersion parameter is useful in comparing distribution means when they (the means) are far apart.<sup>29</sup>

### 3.1.8 Spectral Analysis

Fast Fourier Transform (FFT) analysis was performed on the acquired arc voltage data from the four welding runs. Mathworks Matlab Version 4.2a software was used with minor modifications (Department of Chemical Engineering, U of A) to perform the non-parametric spectral analysis. Better spectral estimates of the acquired data were obtained by using the FFT method together with the Hanning Window. Raw FFT data (i.e. data without windows) showed excessive variance in



the spectral estimates necessitating further smoothing. The frequency of the periodograms ranged from zero to the Nyquist Frequency,  $\pi/T_s$ , where  $T_s$  is the sampling time (0.001 seconds). Appendix B contains Matlab and Unix commands for the spectral analysis.



## **4.0 RESULTS**

Results of the experimentation are presented in this section. Some explanation and interpretation of the findings is also included.

### **4.1 Baseline Power Supply Comparison**

#### **4.1.1 Arc Voltage Calibration**

Significant variance in static voltage existed between the Linde SVI and PowerWave 450 supplies. Compared to the voltage shown on the digital display on the wire feeder, the PowerWave 450 showed a -0.6 V drop at terminals (output stud) and a -2.3 V drop at the arc (Table 4). The PowerWave operators' manual (p/n IM 524) indicates that with an additional Break-out Kit (p/n K948-1), both electrode and workpiece voltage sensing are possible. Without this kit, as was the case in the present research, the PowerWave voltage sensing defaults to terminal sensing. In comparison, the SVI voltage drop was less than 1 V measured at both the terminals and the arc. Both supplies were checked with the same 5.5 m (#3/0) ground cable, therefore, voltage drop can be attributed to the different positive cables. The SVI positive cable was a 3 m (#2/0) copper cable, while a 4.5 m Lincoln Magnum PowerWave Water-cooled gun and cable assembly were used with the PowerWave (prototype Model 400 WC, p/n K684-99). Note the cables used throughout met the requirements of the respective power supply manufacturers.



#### **4.1.2 Spatter Spark Trail Photographs**

Time exposure photographs of Figure 10 show spatter spark trails. No obvious difference existed between the spark trails as a function of base metal. The SVI did however show less spatter generation than the PowerWave 450 on ASTM A36. On IPSCO #426507, both supplies showed comparable amounts of spatter.

Duplicate welding runs and photographs showed somewhat different trends than that of Figure 10. The duplicate run photographs showed #426507 base metal caused fewer spark trails than A36 with both power supplies, and also, the SVI produced fewer spark trails than the PowerWave 450 with both base metals. Unfortunately, these duplicate photographs were taken without blocking the glare of the welding arc and as a result were not report quality. For completeness however, these photographs are included in Appendix D.

#### **4.1.3 Visual Weld Appearance**

Figures 11(a) and 11(b) show completed welds on A36 base metal. Both power supplies produced small, spherical spatter ( $\leq 1$  mm dia.). General weld appearance was satisfactory with no step-like flaws.

Figures 11(c) and 11(d) show completed welds on #426507 base metal. In contrast to A36, the spatter from both power supplies was larger in diameter (2 - 3.5 mm) and lower in total number. Step-like flaws were present in both welds on the #426507 base metal.



#### **4.1.4 Electrode Tip**

Figure 12 shows typical electrode tips following weld runs. On A36 the solidified pendant droplet was spherical and axisymmetric with respect to the electrode wire. Droplet diameter was approximately 3X that on the wire.

On #426507 a much different pendant droplet condition existed. The droplets from both power supplies were laterally displaced and no longer positioned beneath the electrode wire, i.e., solidified upwards and to the side of the wire. Droplet diameter had also increased to approximately 3 - 5X that of the wire.

#### **4.1.5 Data Acquisition**

A key to voltage versus time oscillogram signatures is provided by Figure 13. Experimental oscillograms for the two power supplies and two base metals are shown by Figures 14, 15, and 16. Time spans depicted are 4, 1, and 0.2 seconds respectively.

The 4 second oscillograms of Figure 14 show that both power supplies maintained regular short circuit transfer events on A36. However, on #426507, both supplies showed a marked decrease in SCF. Comparatively, the PowerWave 450 appeared to maintain the set voltage more closely than the SVI with both base metals.

From the 1 second oscillograms of Figure 15, the fundamental difference between the SVI and PowerWave 450 becomes more clear. Both with A36 and #426507 base metals, the quicker response of the PowerWave 450 is apparent as indicated by



sharp changes in voltage over a given time period. With the #426507 base metal, both supplies suffer from a decrease in stability and concomitant decrease in SCF as brought about by extended arc duration.

Extended arc flaring is clearly shown by the representative 0.2 second oscillograms of Figure 16. With both base metals, the SVI showed a slower response as indicated by a less erratic voltage change. The PowerWave 450 also shows a distinctive tendency to minimize instantaneous short circuits, i.e., a higher percentage of total short circuits involves metal transfer.

#### 4.1.6 Statistical Analysis

Statistical analyses were performed on the acquired arc voltage versus time data. Results are depicted by a series of bar charts and histograms. In summary, these are:

##### Bar Charts

- Figure 17: Short Circuit Frequency (SCF)
- Figure 18: Short Circuit Duration
- Figure 19: Instantaneous Short Circuit Ratio
- Figure 20: Arc Duration
- Figure 21: Arc Coefficient of Variation



## Histograms

- Figure 22: Short Circuit Frequency (SCF)
- Figure 23: Short Circuit Duration
- Figure 24: Arc Duration

### **4.1.6.1 Bar Charts**

SCF provides an indicator of the frequency of metal transfer events. The significant decrease in SCF as a function of base metal is clearly shown by Figure 17. In going from A36 to #426507, SVI SCF decreased from 58 Hz to 22 Hz (62%) and the PowerWave SCF from 51 Hz to 14 Hz (73%). The SVI had a higher SCF than the PowerWave 450 with both base metals. Specifically, the SVI SCF was 12% higher on A36 and 58% higher with #426507.

Short circuit duration describes the time interval in which metal transfer is occurring. Figure 18 shows, that with both A36 and #426507, the PowerWave 450 had a longer mean short circuit duration. However, a larger spread in the data existed as depicted by the higher standard deviation (more pronounced with A36). With #426507, both power supplies had similar short circuit duration.

Instantaneous short circuit ratio provides a measure of true metal transfer short circuits as opposed to non-metal transfer short circuits. Figure 19 clearly shows the PowerWave 450 had a lower percentage of instantaneous short circuits with both base metals.



Arc duration is one of the more important parameters to the instability problem since it provides a measure of the amount of arc flaring. Figure 20 shows arc duration was virtually identical for the two power supplies on A36. However, with #426507 arc duration increased significantly and the magnitude of increase was greater with the PowerWave 450 than the SVI. Arc duration standard deviation was also notably higher with the PowerWave 450 than the SVI on #426507.

Figure 21 shows the arc coefficient of variation of the two power supplies with the two base metals. With A36, the relative dispersion from the respective means indicates the PowerWave provided more “regular” arc duration, i.e., lower coefficient of variation. This result is not apparent from the arc duration standard deviation of Figure 20. It is however apparent from the histogram depiction of the same (Figure 23 subsequently discussed). On #426507, the SVI had a slightly lower arc coefficient of variation than the PowerWave 450.

#### 4.1.6.2 Histograms

Histograms depicting short circuit frequency (SCF), short circuit duration, and arc duration provide another perspective on process stability. Figure 22 shows the SCF distribution. The difference in SCF as a function of both base metal and power supply is again apparent as in the bar chart depiction of the same (Figure 17). The SVI clearly showed a less scattered distribution compared to the PowerWave 450 with both base metals. All SCF distributions appeared somewhat normal (Gaussian).



Short circuit duration is shown by Figure 23 and represents true metal transfer events, i.e., instantaneous short circuits are not included. On A36, both power supplies provided a normal distribution with the PowerWave 450 showing a tendency for longer short circuit times. On #426507 the SVI showed a positive skew whereas the PowerWave 450 maintained a normal distribution and again tended towards longer short circuit duration.

Figure 24 shows the arc duration histograms. With A36, the PowerWave 450 had many more intervals between 0.022 and 0.037 seconds than the SVI. By averaging the two adjacent counts of Figure 24(b), the average is approximately that of the SVI on A36. The near identical averages were brought forth on the bar graph depiction of arc duration (Figure 20). Hence, a short coming of the bar graph approach is apparent. The histogram approach clearly differentiates between arc duration distribution, whereas the bar graphs did not. The preponderance of 0.020-0.035 second arc intervals of the PowerWave is also consistent with a lower arc coefficient of variation (Figure 21).

On #426507, the SVI showed a positively skewed arc duration distribution with very little scatter. In comparison, the PowerWave 450 had a much wider distribution and was somewhat Gaussian. The PowerWave histogram dispersion is consistent with the higher standard deviation in arc duration (Figure 20) and higher arc coefficient of variation (Figure 21).



#### 4.1.7 Spectral Analysis

Periodograms of the acquired voltage data from the four-weld test matrix are shown by Figure 25. The periodograms show both power supplies underwent a reduction in peak frequency and a decrease in power density with IPSCO #426507 compared to A36. Furthermore, on A36 both supplies' spectra were somewhat "h" shaped indicating a secondary peak frequency while on #426507 this prominent feature was not present.

The peak frequencies corresponding to the maximum power spectral density for each of the four welds are summarized by Table 5. Noteworthy is the 60% reduction in peak frequency of the SVI compared to a 17% reduction with the PowerWave in going from A36 to #426507.

The spectral peak frequencies of Table 5 were converted to cycles/second (Hz) (see Appendix C for sample calculations). Figure 26 compares the results of LabVIEW generated SCF (same as Figure 17) and the Matlab FFT pseudo SCF. The PowerWave on A36 and the SVI on #426507 appeared to correlate well, however, significant difference existed between the SVI on A36 and PowerWave on #426507.

In addition a reverse trend in the SCF emerged. In time domain the SVI showed a higher SCF than the PowerWave for both base metals, whereas in frequency domain, the PowerWave SCF was higher for both base metals.

*Parametric* spectral analysis methods were briefly investigated. The parametric method constructs a spectrum from the parametric model of the signal rather than directly from the data signal itself, i.e., a synthetic spectrum is constructed.



Appendix E shows the results of the Linde SVI on A36. The parametric results can be compared to the non-parametric depiction of the same data (Figure 25). However, for direct comparison of the non-parametric and parametric results, additional frequency adjustments would be necessary. Even with these frequency adjustments, the shape of the spectral distribution should not change. Further investigation into parametric analysis of GMAW-S data would be an obvious research extension, since in itself, the method represents the latest technology for digital signal processing.



## **5.0 DISCUSSION**

The results of arc voltage calibration, spatter spark trail photographs, visual weld appearance, electrode tip morphology, data acquisition, statistical analysis, and spectral analysis are discussed in this section. The significance of the same to arc instability phenomenon is brought forth. From the identified high information content parameters specific to arc instability, a performance comparison of the two power supplies then follows. The section concludes by comparing the relative severity of arc instability predicted by the instability formula of Equation (1) to the experimental results.

### **5.1 Baseline Power Supply Performance**

#### **5.1.1 Arc Voltage Calibration**

With the PowerWave 450, significant variance existed between the LED display voltage and measured arc voltage. The voltage drop is associated with the gun and cable assembly and does not present a problem if the user is aware of the condition. Arc voltage should be checked to ensure adherence with procedural requirements, and where possible, static methods be used.



Alternatively and preferably, an optional Break-out Kit (p/n K948-1) can be used. However, even with the additional leads in place, results suggest a 0.5 V voltage drop may still exist between the display voltage and the actual arc voltage. Therefore, static calibration should still be initially performed.

### **5.1.2 Spatter Spark Trail Photographs**

The spatter spark trail photographs were considered a “quick and easy” method to quantify the amount of spatter generated during welding. Unfortunately, inconsistency existed between the two sets of spatter spark trail photographs. It appears that a one second exposure time may be insufficient to provide reproducible spark trail results.

The initial set of photographs clearly showed less spatter generated with #426507 than with A36. This trend fits the spatter morphology of the final welds and the acquired arc duration data considerably better (subsequently discussed).

### **5.1.3 Visual Weld Appearance**

Final weld profiles showed step-like flaws in the #426507 welds while the A36 welds had a smooth profile. Literature suggests these flaws originate from too much metal being deposited per transfer event due to an extremely extended period between short circuits. The advancing solidification front of the solid/liquid interface, located at the rear of the molten pool, then “freezes in” the excess volume of electrode material.<sup>19</sup> Consistent with literature, our experimental oscillograms



and statistical analysis of arc duration clearly showed extended arcing periods with #426507 compared to A36.

Large diameter spatter was present on the surfaces of the #426507 welds. Extended arc duration allows the pendant droplet at the tip of the electrode to increase in size before being ejected as spatter. One of two sets of spatter spark trail photographs provided visual evidence of a decreasing amount of spatter with #426507. In contrast, welding on A36 produces much finer spatter since total arcing time is less.

No significant difference existed in the visual appearance of the welds made on either base metal as a function of power supply.

#### **5.1.4 Electrode Tip**

Both power supplies showed near identical solidified pendant droplets on the respective electrode tips for both base metals. Photographs of the pendant droplets clearly showed evidence of a repulsive force in play with #426507. The force is obviously extremely violent and large enough in magnitude to eject pendant droplets as spatter. It is likely the cause of the repulsive force is “reverse plasma jets” as explained in the Literature Review section of this report (2.2.2 Arc Physics). In contrast, on A36 the pendant droplet was much smaller in diameter and axisymmetric with respect to the electrode wire.



### **5.1.5 Data Acquisition**

Oscillograms generated from the voltage versus time data acquired during welding provide one medium of characterizing process stability. The graphical depiction readily shows the difference between stable (A36) and unstable (#426507) welding conditions. Stability in the sense of GMAW-S is a relative term. The 0.2 second oscillograms most clearly showed the arc flaring phenomenon.

### **5.1.6 Statistical Analysis**

Two approaches for quantifying process stability in time domain were used; bar chart comparisons and histograms. Results indicate some of the statistical parameters are more valuable than others depending on the desired use, i.e., process stability as a function of base metal or process stability as a function of power supply. By considering the relative difference in the respective statistic, and a contemplative grading system, a summary Table was constructed. From Table 6, the most valuable parameters and their method of depiction for arc instability influenced GMAW-S are:

- Arc Duration (bar chart)
- SCF (histogram)
- Arc Duration (histogram)
- FFT Spectrum (subsequently discussed)

The above parameters appear to provide the most sensitivity for extended arc duration phenomenon which was shown by oscillograms to be the most discernible



difference when welding on #426507. These identified parameters should provide the best “yardstick” for quantifying power supply performance, i.e., PowerWave waveform development.

### 5.1.7 Spectral Analysis

#### 5.1.7.1 Background to Spectral Analysis

Spectral analysis of welding data represents a relatively new method for process examination, consequently, a brief overview is warranted at this point. Spectral analysis attempts to detect underlying periodic components of a function in time domain,  $x(t)$ , by computing its power spectrum. The power spectrum shows an average distribution of energy in  $x(t)$  among different frequency components.<sup>31</sup>

Evaluating equation (5) generates the periodogram.

$$P_k = \frac{1}{N} \left| \sum_{i=1}^{N-1} x_i \omega_i e^{(-j2\pi k i)} \right|^2 \quad (5)$$

where:  $P_k$  = discrete power spectral density

$N$  = number of samples

$\omega_i$  = window function

$j = \sqrt{-1}$



In this experimentation, a Hanning window was used which is defined as:<sup>32</sup>

$$\omega_i = 0.5[1 - \cos(2\pi \frac{n}{n+1})] \quad (6)$$

where:  $n = 1 \dots N$

With  $N$  equal to 4000, a total of 47,900 computations were required to perform the Fast Fourier Transform (FFT) and generate the periodogram. Note that with a Discrete Fourier Transform (DFT), some 16 million calculations would have been required.<sup>33</sup> The window function smoothes out short term fluctuations before transformation into the frequency domain, i.e., it eliminates harmonic components whose periods are not integer factors of the analysis interval. The effect is to reduce the variance of the spectral estimate.<sup>32</sup>

There are four basic requirements which have to be met in the design of a spectral analysis:<sup>34</sup>

- 1) It is necessary to sample the signal at a rate greater than twice the highest frequency of interest in the signal spectrum. The highest frequency that can be recovered in a digital signal is  $\pi/T_s$  which is the Nyquist Frequency. For GMAW-S with a SCF in the order of 60 Hz, the sampling rate should be no less than 120 samples per second. This required rate equates to a maximum sampling interval of no greater than 0.008 seconds. Note that in our experimentation the sampling interval was 0.001 seconds.



- 2) Care must be taken to avoid aliasing. With GMAW-S, this is accomplished by adhering to the sampling rate or interval criterion. If the source signal contains frequencies higher than those of interest in the data analysis, i.e., higher than the Nyquist Frequency, then an “anti-aliasing” filter should be used to eliminate these frequencies by “low pass filtering” the experimental analog signal.
- 3) The truncation point of the spectrum must be such that the bandwidth is less than the width of the narrowest important peak in the spectrum.
- 4) The data acquisition time span must be greater than  $v/2a$ , where “ $v$ ” is the degrees of freedom and “ $a$ ” is the detail width of the spectrum. For example, in GMAW-S, “ $v$ ” can be chosen as 30 and “ $a$ ” as, say, 400 radians/second (64 Hz). At least 0.25 seconds of acquired data would then be required. Note in this experimentation four seconds of voltage data was acquired.

Applications of FFT to welding data are scarce in published literature. Probably the best application was the work by Wang *et al.*<sup>26</sup> in which metal transfer modes were characterized in FCAW. They reported success with spray and globular transfer but marginal success with short circuit transfer. A periodic structure could not be discerned in their experimentation with short circuit transfer.

### 5.1.7.2 Spectral Analysis Interpretation

Spectral analysis distinctly showed a difference among the four welds of the test matrix. As such, the method provides another window of observation on the welding process. The single most important parameter that can be obtained from



the spectral analyses is the peak frequency. In GMAW-S, the higher the frequency - - the greater the number of periodic events, i.e., metal transfer.

The spectral analysis results were comparable to the time domain results. In itself, this result provides some confidence in the respective “black boxes.” The fact that better correlation between the two domains was not realized should not be an issue. Smoothing coefficient selection plays an important role spectral analysis. SCF correlation could have been easily obtained by “adjusting” the spectral analysis smoothing coefficient had correlation been the objective. However, for consistency of comparison the same coefficient was used for all spectral analyses.

According to the spectral analysis the PowerWave performance was superior to the SVI. The peak frequency was higher for both base metals and the amount of reduction in frequency in going from A36 to #426507 much less. In contrast, time domain analysis of SCF showed the SVI performance to be superior. Speculatively, this reverse trend may be a function of the response characteristics of the respective power supplies, i.e., the PowerWave responds more quickly and thus tends to promote a higher spectral SCF.

The power density, or magnitude, of the spectra is not a high information parameter. It merely indicates the change in voltage occurring at the respective frequencies. The four second oscilloscopes showed the PowerWave’s change in peak-to-peak voltage ( $\Delta V$ ) to be greater than that of the SVI, ergo, a higher power density.

Given the distinctive differences in the periodograms as a function of power supply and base metal, the spectral analysis method is considered to be a valuable means of quantifying process stability. An obvious application would be in waveform



development. For example, process improvement could be measured by observing the relative spectral distribution compared to the baseline conditions of this research.

### 5.1.8 Overall Performance Comparison

By using the high information content parameters identified in sections 5.1.6 and 5.1.7, baseline performance comparisons of the two power supplies can be made. Criteria for comparison were based on relative power supply response and the effect of introducing an unstable base metal (#426507). If the power supply was superior in one of the preceding two criteria then one ✓ was awarded. If superior in both criteria then two ✓✓ were awarded.

Considering the bar chart depiction of arc duration, no significant difference on A36 existed between the two supplies. However, on #426507, the PowerWave underwent a greater increase in arc duration than the SVI. Hence, the SVI was considered to perform better given extended arc duration is not desirable and was awarded one ✓.

Considering the histogram depiction of SCF on A36, the SVI showed less spread in the range of frequencies and also a higher peak frequency. On #426507, the SVI again showed a narrower distribution and a higher peak frequency. Thus a total of two ✓✓ were awarded to the SVI.



Considering the arc duration histogram on A36, the PowerWave showed a more uniform distribution and was awarded one ✓. However, on #426507 the SVI showed less scatter and awarded one ✓.

Spectral response on both A36 and #426507 favored the PowerWave since higher peak frequencies occurred. Hence, two ✓✓ were awarded to the PowerWave.

Table 7 summarizes the findings of the preceding evaluation. On the baseline comparison of the two power supplies, i.e., no waveform development with the PowerWave, the Linde SVI performed slightly better. With A36, both supplies performed comparably, however, on #426507 the SVI showed more indication of process stability than the PowerWave 450. Inherent process control characteristics of the respective power supplies is likely the reason for the above differences. The SVI has no ability to compensate for changes in the arc resistance, whereas the PowerWave attempts to maintain constant voltage as resistance decreases. In the context of arc instability, it appears that the “unmodified,” fast-reacting PowerWave 450 is more susceptible to arc perturbations than the non-reactive SVI.

## 5.2 Instability Formula

Previous research work at the U. of A. developed a linear regression formula to predict the severity of arc instability based on the chemical composition of the base metal.<sup>7</sup> With A36, the formula predicted a reasonably high and stable SCF, consistent with experimental results. However, with IPSCO #426507 the formula predicted a reduction of approximately 50% in the SCF ( $\approx$ 29 Hz). The actual



experimental results of 22 Hz and 14 Hz for the Linde SVI and PowerWave respectively.

With the SVI, the variation between predicted and experimental SCF's for the #426507 base metal is considered reasonable (-12%). However, with the PowerWave, the rather large variation (-44%) may indicate a power supply specific limitation of the formula. Note that some discrepancy between predicted and actual SCF's can be expected given that the formula was originally developed for a using the Linde SVI and "modified" hot pass parameters, i.e., reduced voltage, wire feed speed and travel speed.



## **6.0 CONCLUSIONS**

1. Key arc instability time domain tools for quantifying GMAW-S process performance were identified as: oscillograms, arc duration bar charts, SCF histograms, and arc duration histograms.
2. Spectral analysis using a Fast Fourier Transform (FFT) was successfully used to identify process stability in GMAW-S. No account of similar work was encountered in the literature sources reviewed.
3. On ASTM A36 both power supplies performed comparably and produced satisfactory welds. On IPSCO GR483 pipeline steel (Heat #426507), both power supplies showed extensive arcing periods with associated large diameter spatter and produced welds with step-like flaws. Process stability on IPSCO #426507 was marginally better with the Linde SVI than the Lincoln PowerWave 450. Inherent process control characteristics of the respective power supplies is likely the reason for the above differences.
4. The PowerWave 450 LED voltage was approximately -0.5 V low as measured at the terminals. Without workpiece or electrode voltage sensing hardware this translated to a -2.3 V drop at the arc. Corrective manipulation of voltage settings enabled meaningful performance comparisons to be made.
5. Spark trail photographs were not very effective in quantifying the amount of spatter.



## 7.0 RECOMMENDATIONS

1. Future work with the PowerWave 450 should incorporate an optional Break-out Kit (p/n K948-1). Voltage sensing at either the electrode or the workpiece could then be implemented.
2. Future arc instability research should make use of both time and frequency domain analysis methods. Oscillograms, arc duration bar charts and histograms, SCF histograms, and FFT spectra are recommended high information content parameters.
3. Data acquisition time should be increased from four to ten seconds while maintaining a sampling interval of 0.001 seconds. The primary benefit would be in time domain histograms, and to a lesser extent, in frequency domain analyses.
4. Conversations with an Application Engineer from Lincoln Electric brought to light the fact the PowerWave process control is based primarily on *current* change. In the present work *voltage* based parameters were used throughout. Although voltage will still provide a means of quantifying improvements in process stability, current based parameters may provide more meaningful information.
5. *Parametric* spectral analysis methods represent another frequency domain digital signal processing technique that may prove beneficial in studying GMAW-S since smoother periodograms are produced compared to non-parametric methods.



## **8.0 TABLES**



Element	ASTM A36 (Nominal)	IPSCO GR483 #426507	IPSCO GR483 #439287 <sup>*1</sup>
C	0.25 max.	0.055	0.039
Mn	0.80-1.20	1.45	1.60
S	0.05 max.	0.002	0.004
P	0.04 max.	0.011	0.013
Si	0.40 max.	0.18	0.262
Cu		0.27	0.258
Ni		0.12	0.122
Cr		0.08	0.082
V		0.002	0.007
Cb		0.067	0.067
Mo		0.19	0.192
Sn		0.018	0.011
Al		0.033	0.032
N		0.0078	0.0104
Ti		0.023	0.025
Ca		0.0062	0.0032
Ce		0.0024	0.0082
B			0.0004
O		0.0024	0.0059

\*1: IPSCO GR483 Heat #439287 was not used for this phase of the research.

**Table 1: Base metal composition (wt%).**



Parameter	Current Nova Procedures	Actual Experimental Runs
Wire <sup>*2</sup>	Thyssen K-Nova	Thyssen K-Nova
Wire Diameter (mm)	0.9	0.9
Shielding Gas	100% CO <sub>2</sub>	100% CO <sub>2</sub>
Gas Flow Rate (m <sup>3</sup> /hr)	2.10	0.9 (15 l/min)
Arc Travel Speed (mm/min)	1270	1270
Wire Feed Speed (mm/min)	12700	12330
CTWD (mm) <sup>*3</sup>	8.9	9
Voltage	23.0 - 26.0	24.3
Amperage	220 - 270	SVI = 220 (default), PW = default
Head Angle	6 degree lead	6 degree lead

\*2: See Appendix A for manufacturer certificate.

\*3: CTWD = Contact Tube to Work Distance.

**Table 2: Hot pass welding parameters.**



Power Supply	Set (mm/min) <sup>*4</sup>	Measured (mm/min)	% Error
Linde SVI	12700	12319	-3.0
PowerWave 450 <sup>*5</sup>	12700	12929	1.8
PowerWave 450 <sup>*5</sup>	12243	12344	+0.8

\*4: 12700 mm/min = 500 in/min.

\*5: Synergic 7 wire feeder.

**Table 3: Wire feed speed calibration.**

Power Supply	Cable Length (ft)		Variance From V <sub>SET</sub> <sup>*6,7</sup>	
	(+)	(-)	Terminal (V)	Arc (V)
Linde SVI	10	18	+0.1	-0.7
PowerWave 450	14	18	-0.6	-2.3

\*6: Linde SVI set voltage = 25 V.

\*7: PowerWave 450 set voltage = 26.5 V.

**Table 4: Arc voltage calibration.**

Power Supply	A36	IPSCO #426507	Reduction
Linde SVI	249.3	99.7	60%
PowerWave 450	299.2	249.3	17%

**Table 5: Spectral analysis peak frequencies.**



Parameter	Comparison		
	Base Metal	Power Supply	Value
SCF	✓✓	~	★★½
SC Duration	~	~	★
Instantaneous SC Ratio	~	~	★
Arc Duration	✓✓	✓	★★★
Arc Coefficient of Variation	✓	✓	★★
SCF (histogram)	✓✓	✓✓	★★★★
SC Duration (histogram)	~	✓	★½
Arc Duration (histogram)	✓✓	✓✓	★★★★
FFT Spectrum	✓✓	✓✓	★★★★

**Table 6: Process Characterization Parameters for GMAW-S.**

Parameter	Power Supply Performance <sup>*8,9</sup>	
	Linde SVI	PowerWave 450
Arc Duration (bar chart)	✓	
SCF (histogram)	✓✓	
Arc Duration (histogram)	✓	✓
FFT Spectrum		✓✓
Total	4✓	3✓

\*8: ✓ = Superior in one of power supply or base metal comparison criteria.

\*9: ✓✓ = Superior in both power supply and base metal comparison criterion.

**Table 7: Overall power supply performance based on arc instability criteria.**



## **9.0 FIGURES**



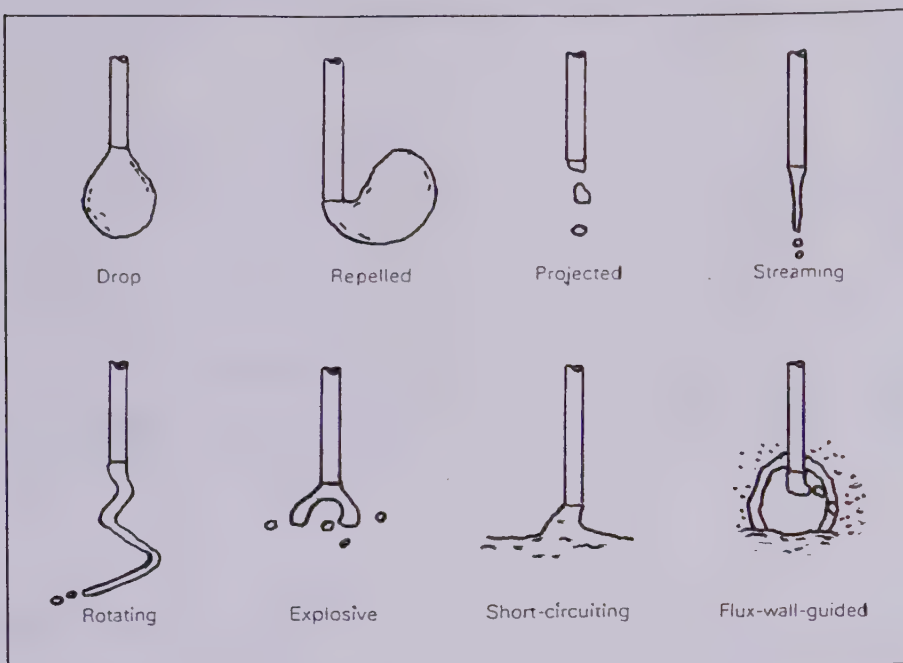


**Figure 1: Metal transfer modes in arc welding.<sup>1</sup>**

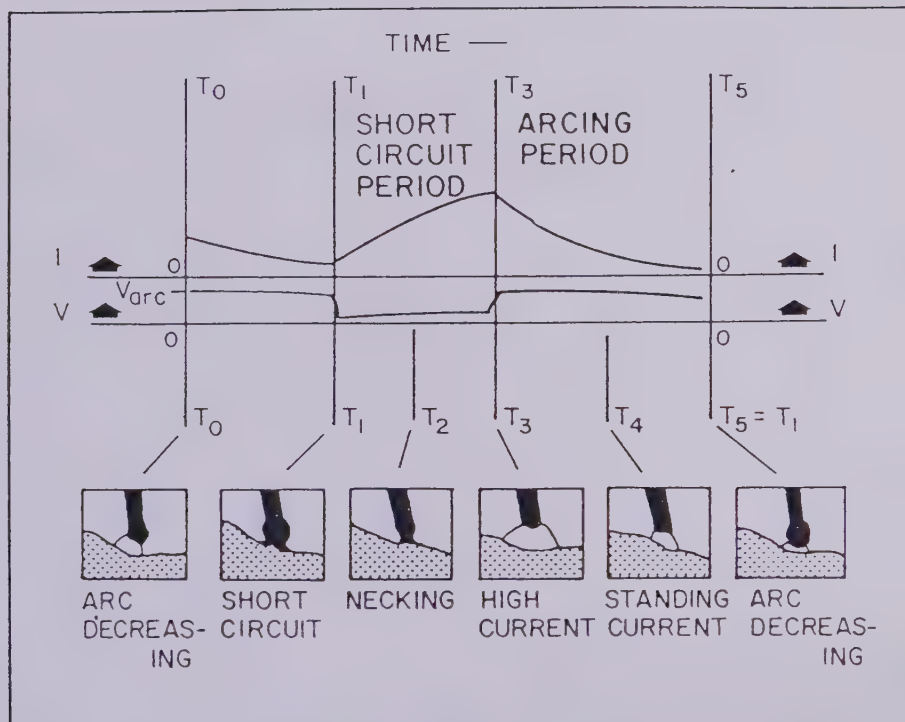
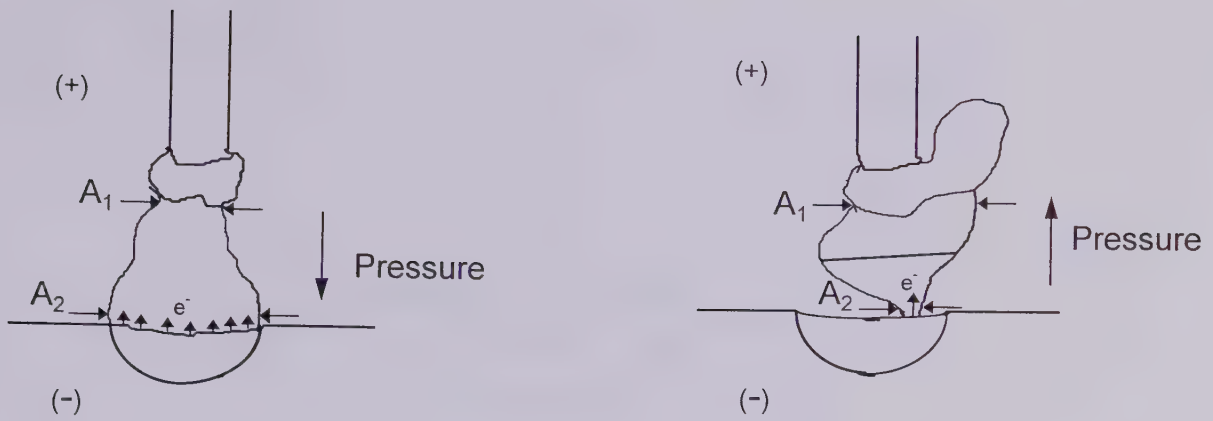


**Figure 2: Instantaneous arc voltage and current variation during short-circuiting transfer.**





(a) Stable arc.  $A_1 < A_2$ .

(b) Unstable arc.  $A_1 > A_2$ .  
Reverse plasma jets  
form and arc pressure  
is reversed.

Figure 3: Schematic representation of stable and unstable arcs.

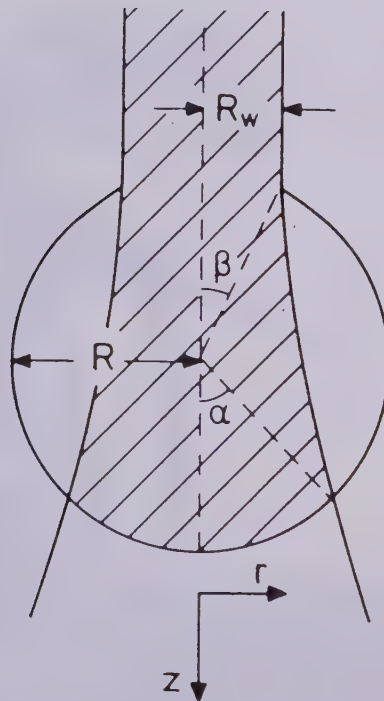


Figure 4: Arc pressure as a function of droplet dimensions.  
Upward pressure results when angle  $\alpha < \beta$ .





**Figure 5:** Mode 1 weld pool oscillation.<sup>18</sup>



**Figure 6:** Typical base metal and strongback assembly.



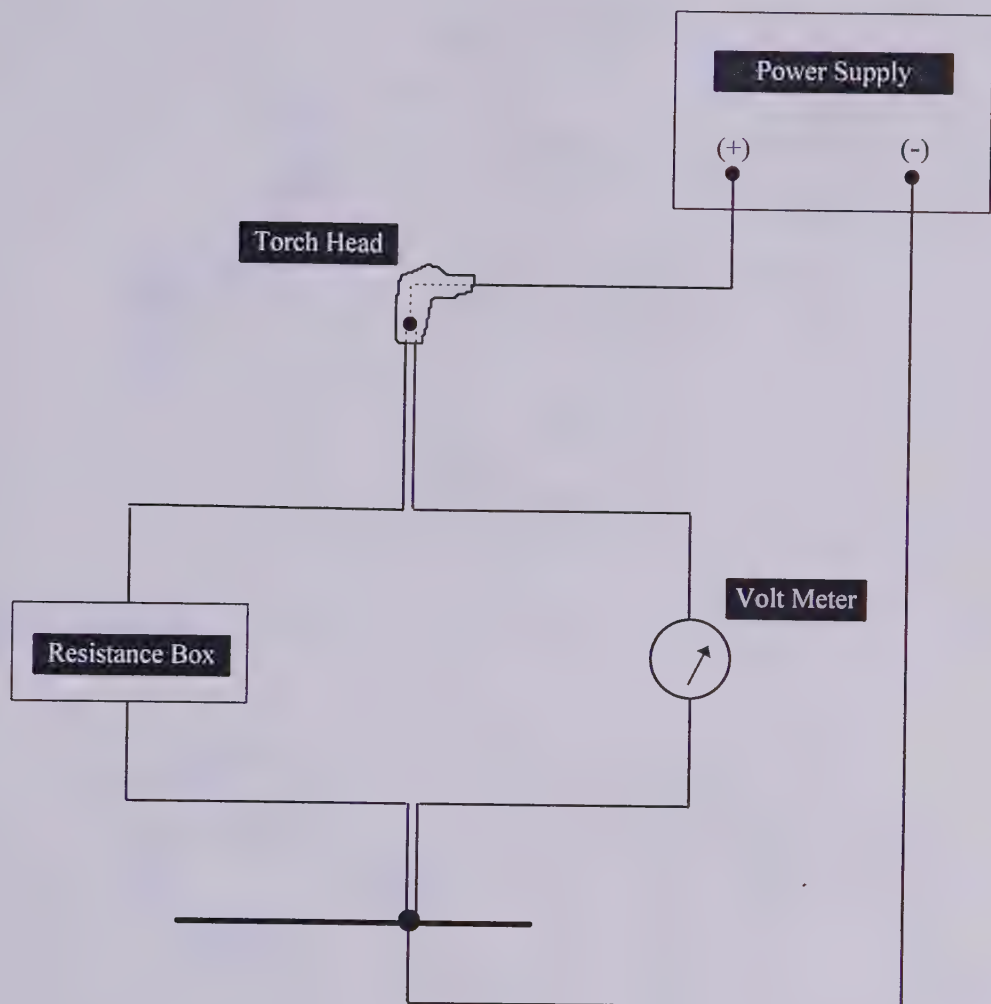
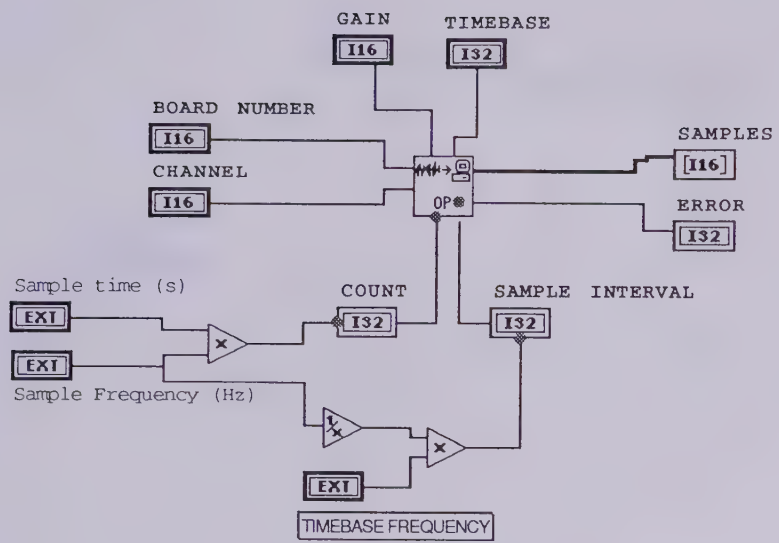
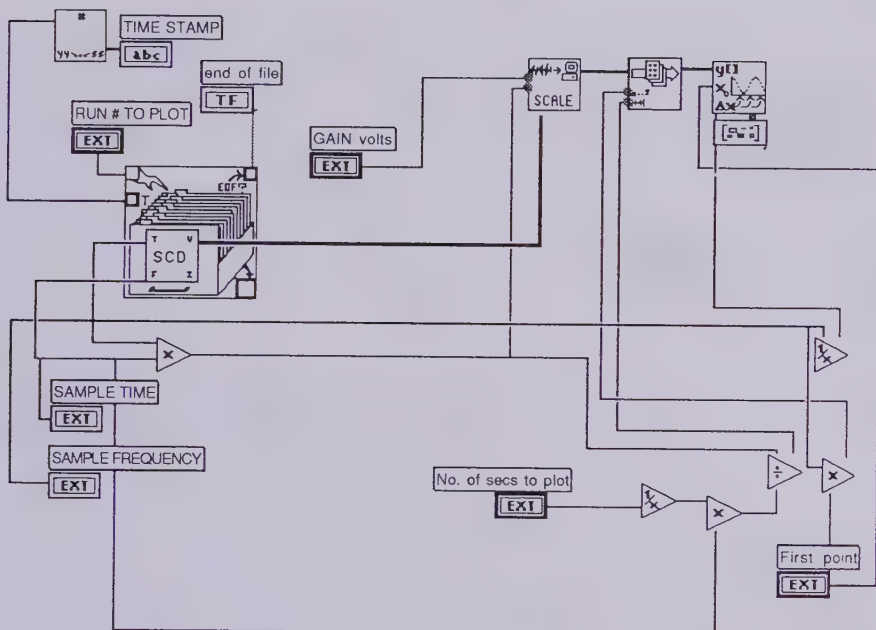


**Figure 7: Static resistance arc voltage calibration.**





(a) Acquisition.



(b) Analysis and plotting.

**Figure 8: Data acquisition virtual image block diagram.**



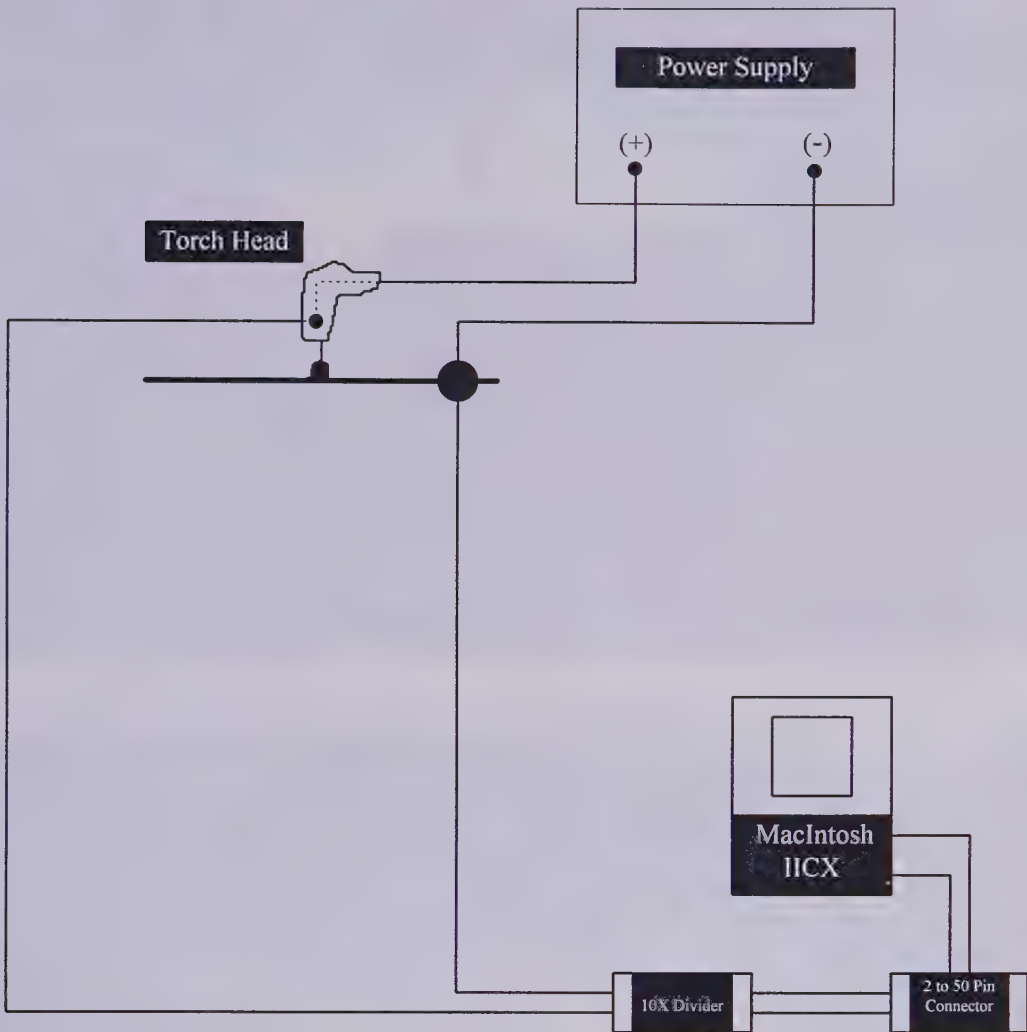
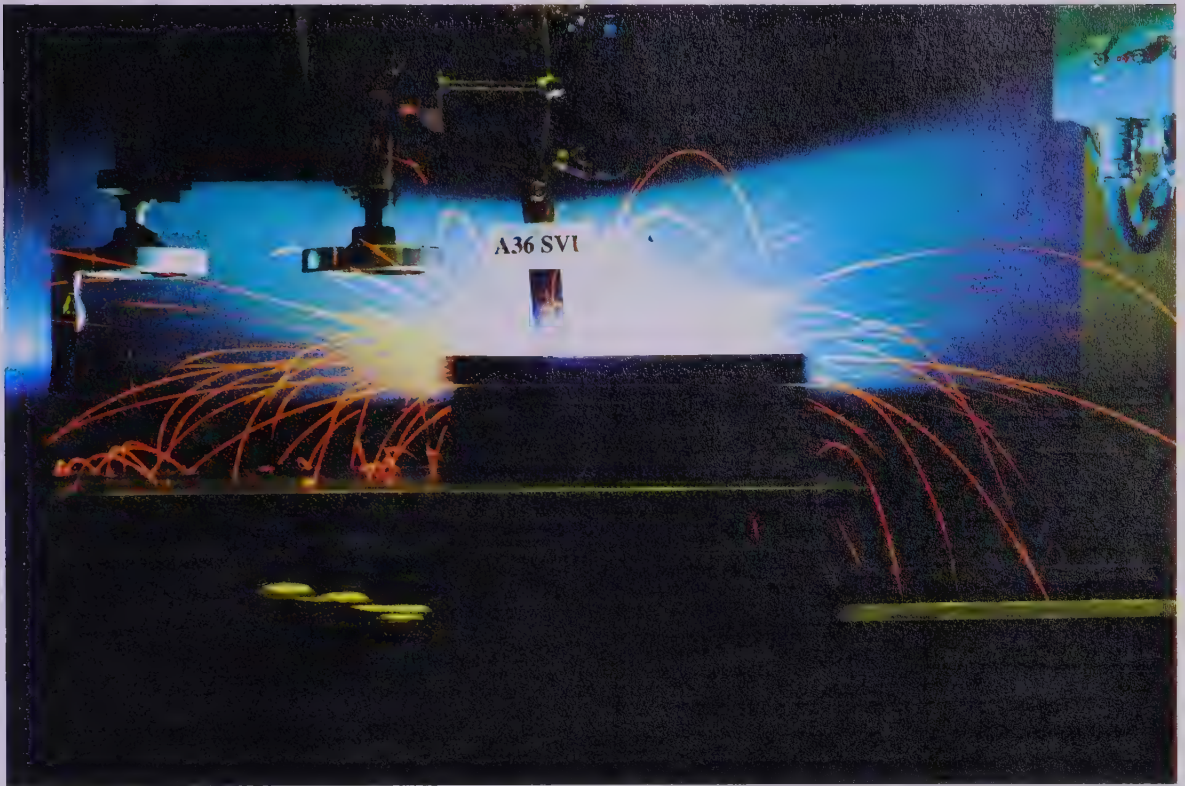
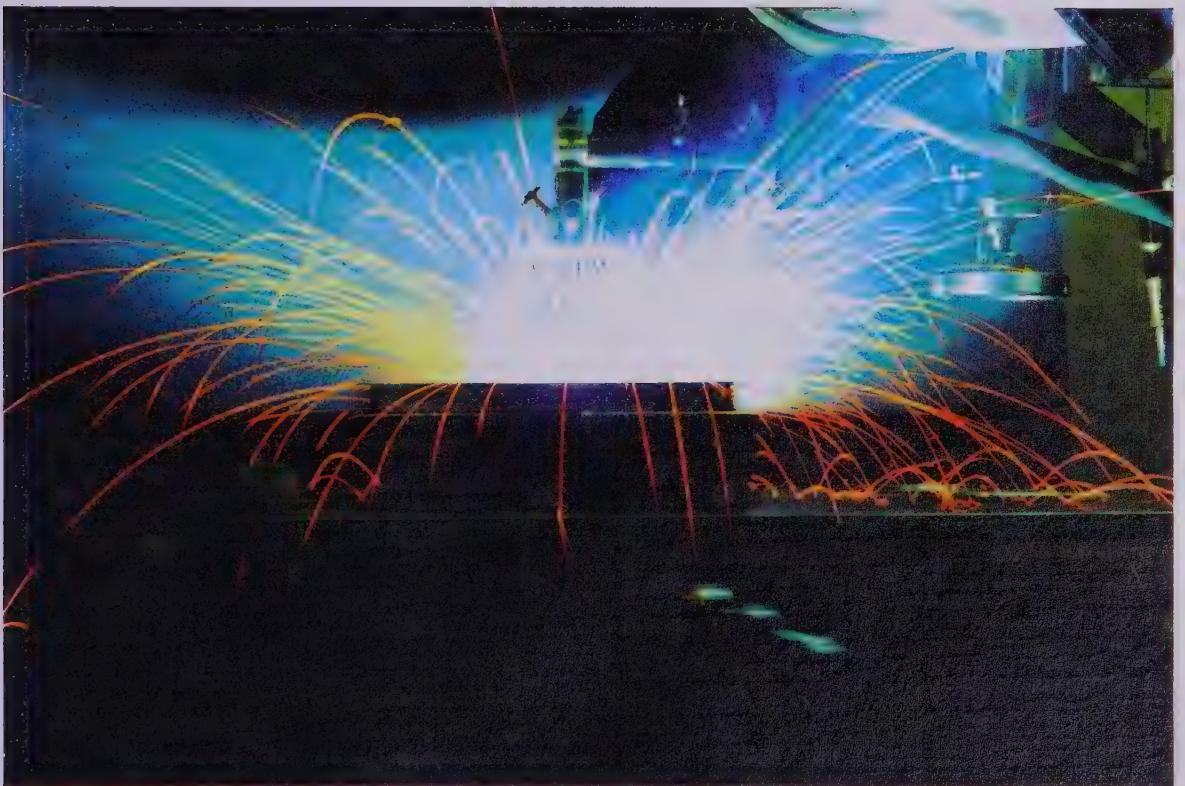


**Figure 9: Data acquisition set-up.**





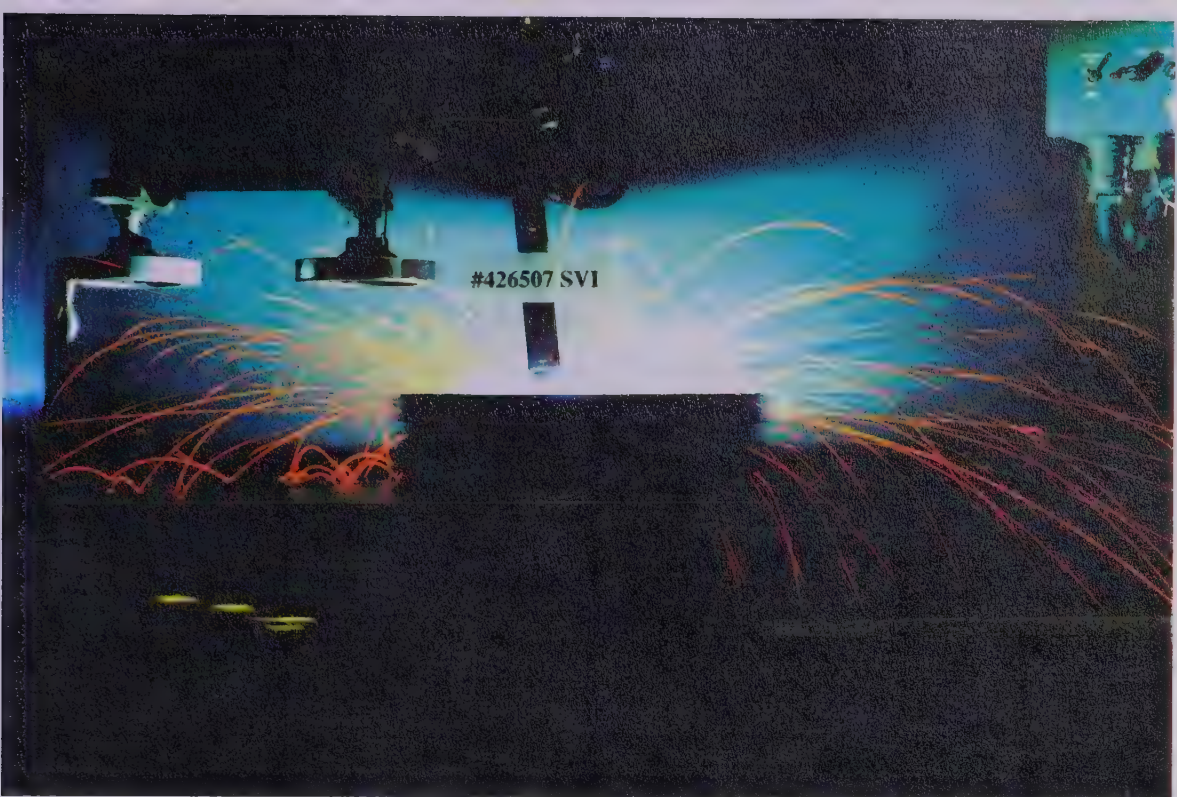
(a) SVI on A36.



(b) PowerWave 450 on A36.

**Figure 10: Spatter spark trails.**





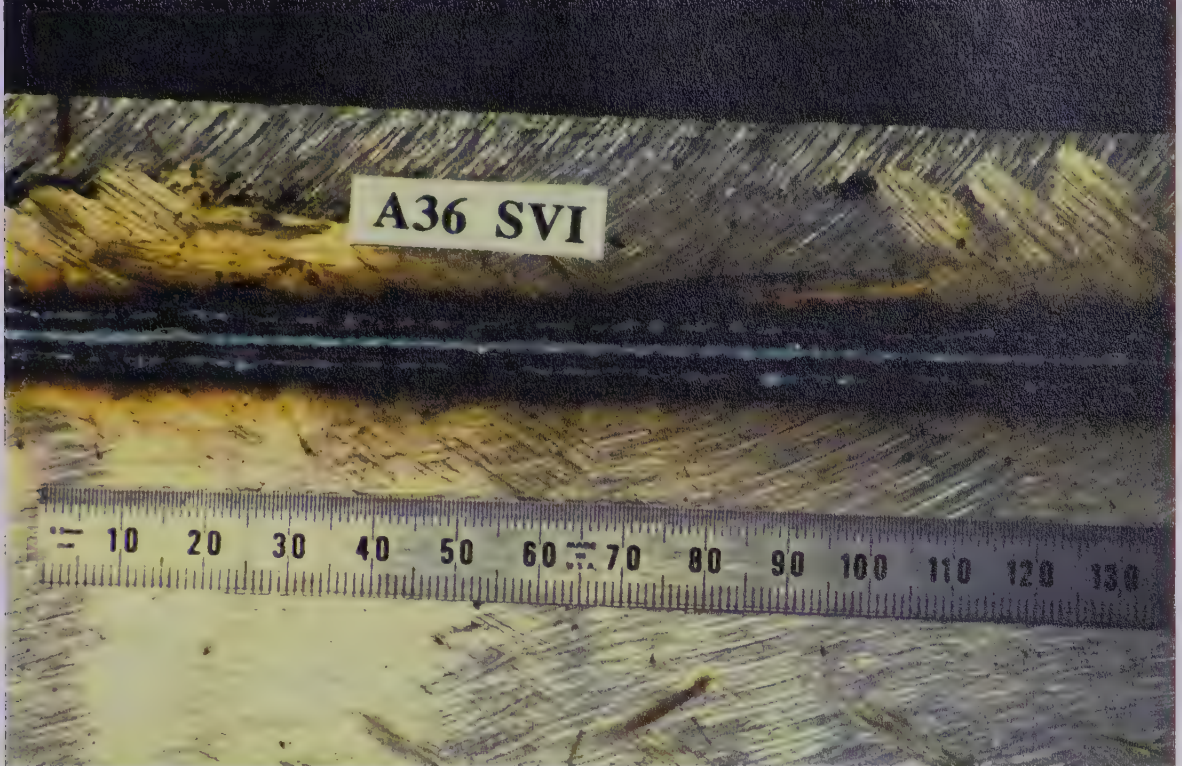
(c) SVI on #426507.



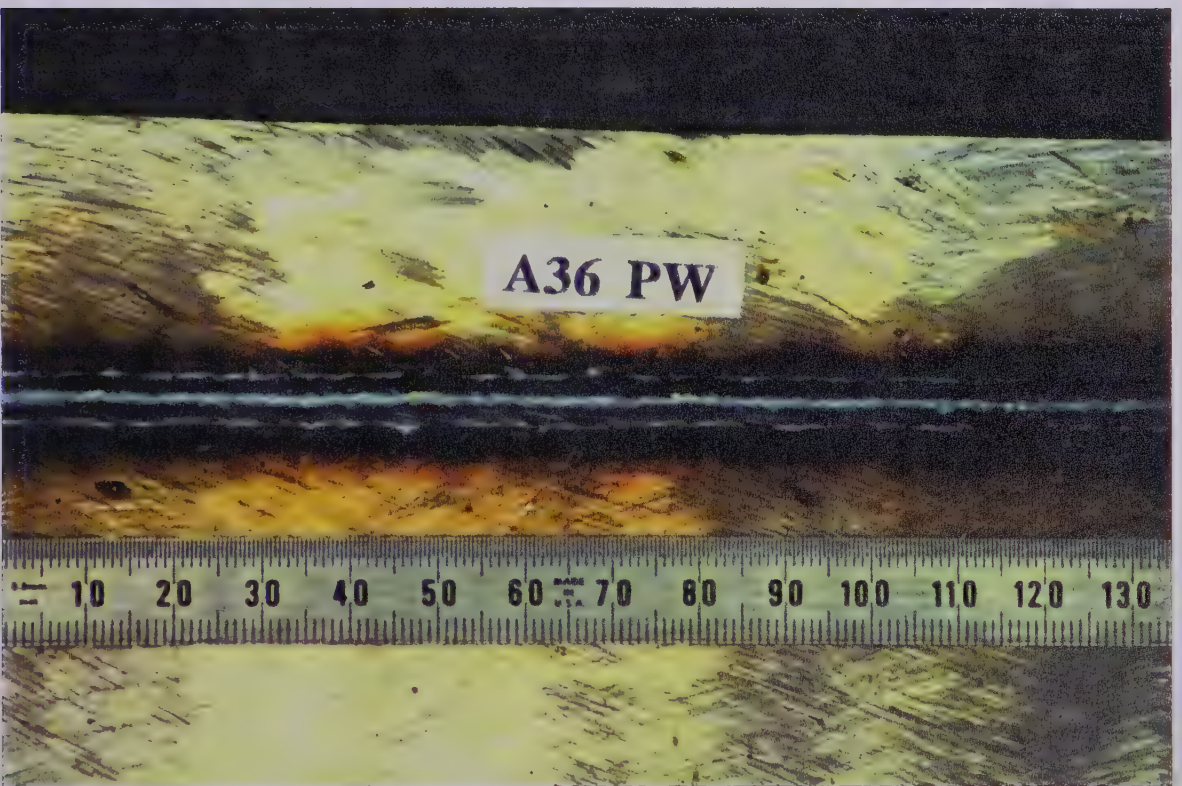
(d) PowerWave 450 on #426507.

**Figure 10: Spatter spark trails.**





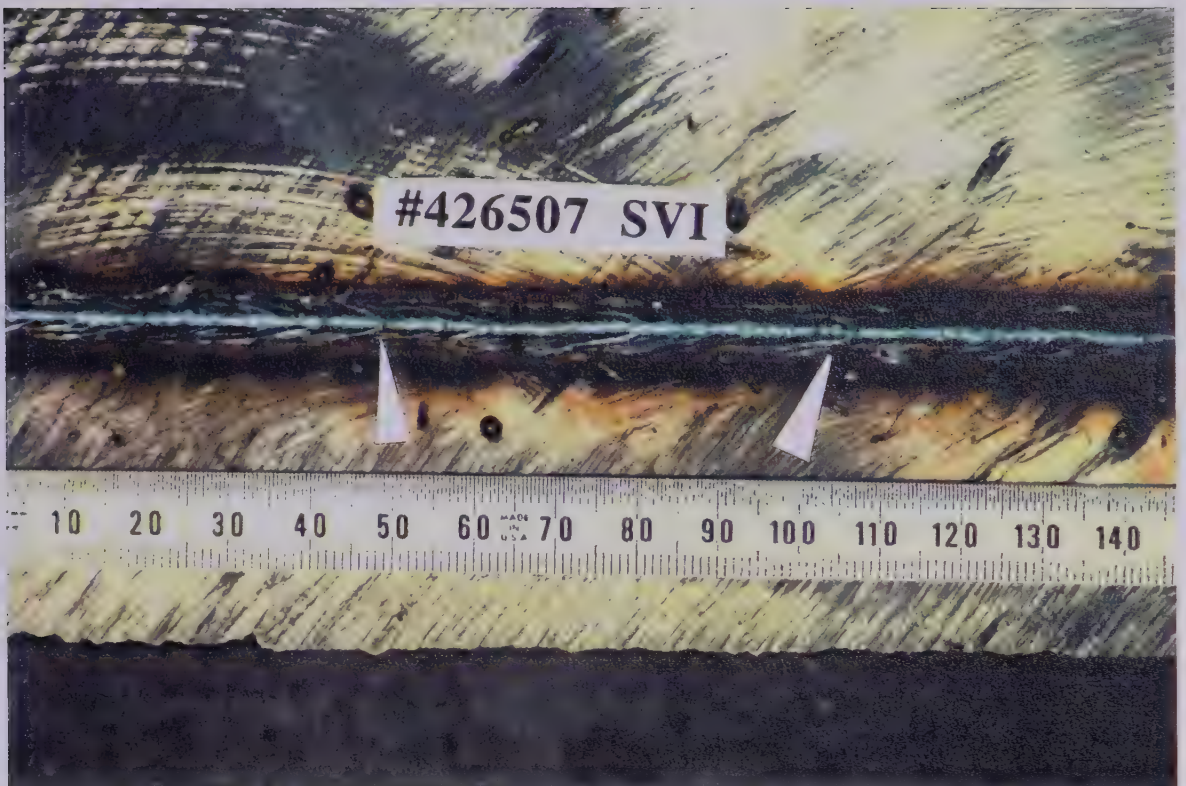
(a) SVI on A36.



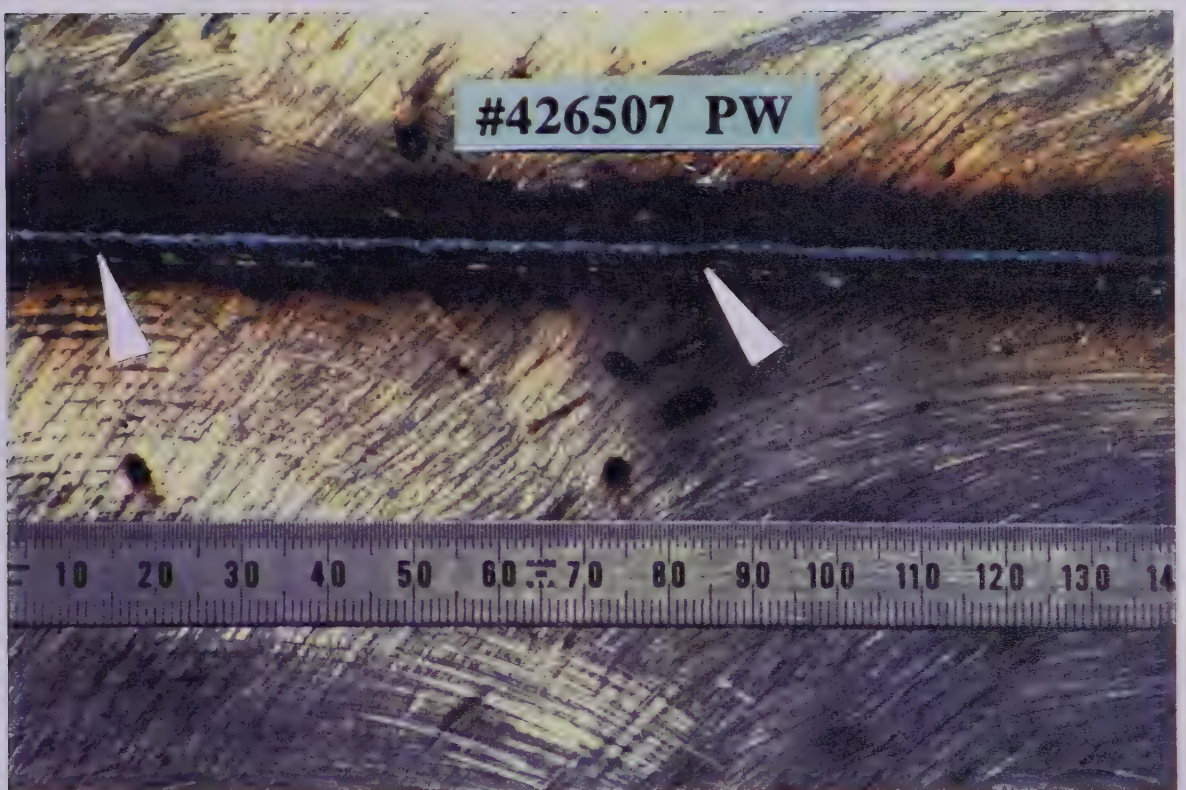
(b) PowerWave 450 on A36.

**Figure 11: Completed welds.**





(c) SVI on #426507.



(d) PowerWave 450 on #426507.

**Figure 11: Completed welds. Arrows indicate step-like flaws.**



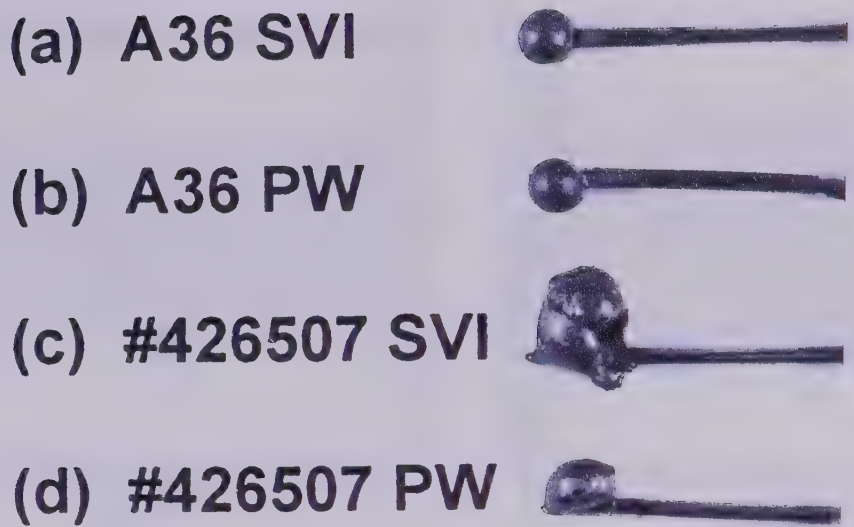


Figure 12: Electrode tips.

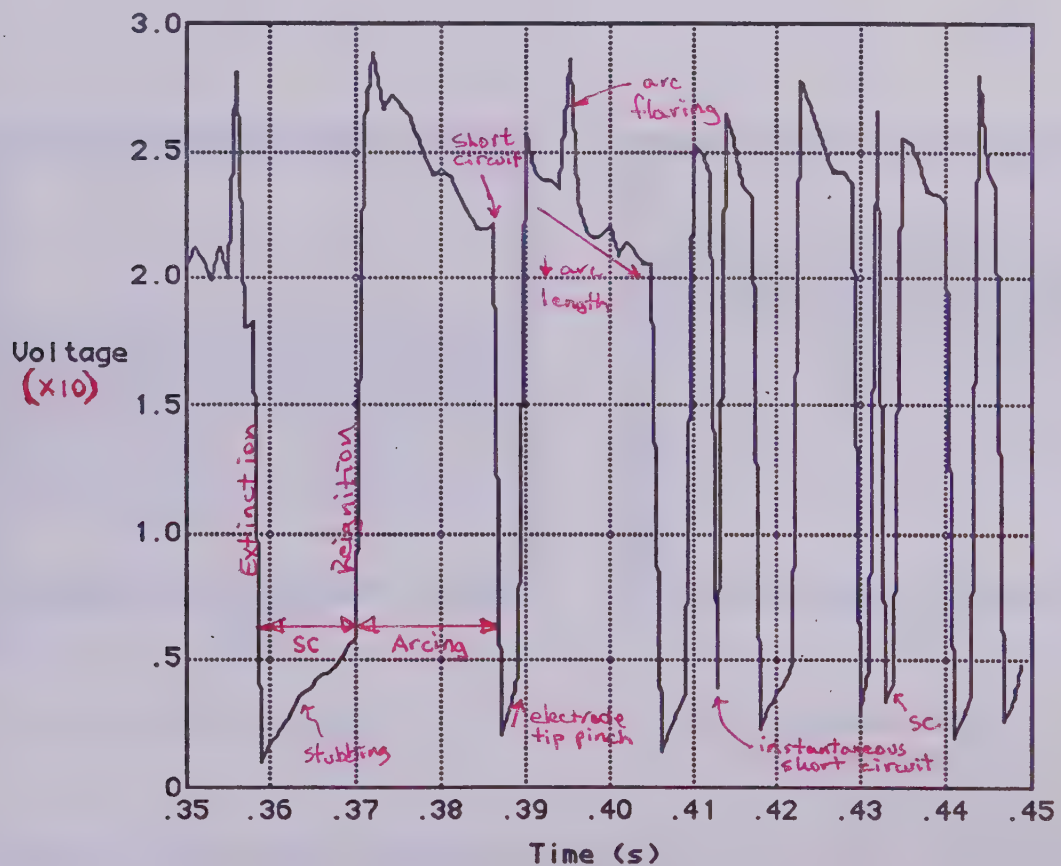
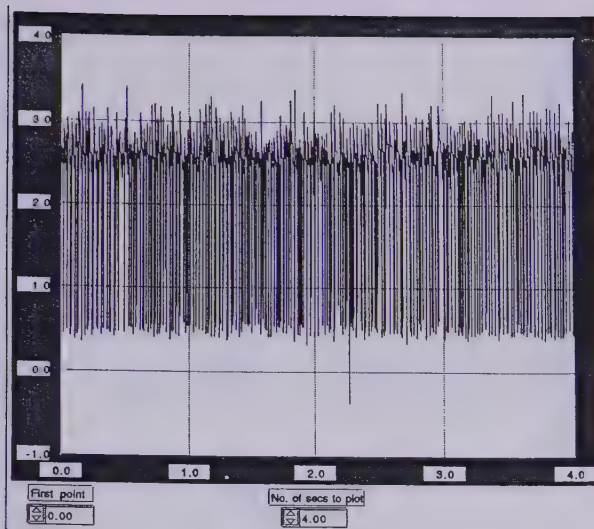
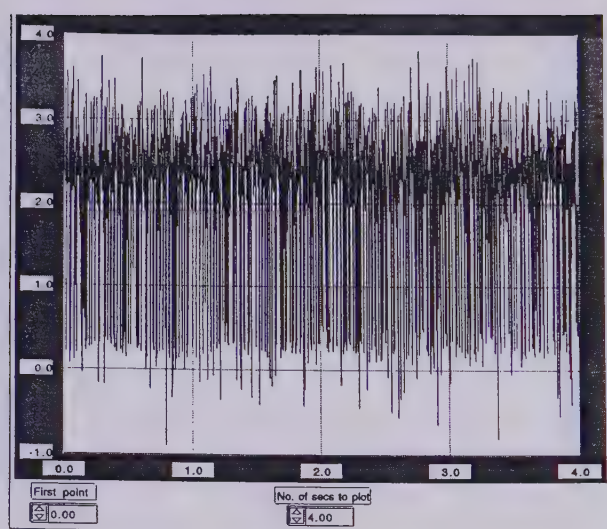


Figure 13: Key to oscillogram signatures.<sup>30</sup>

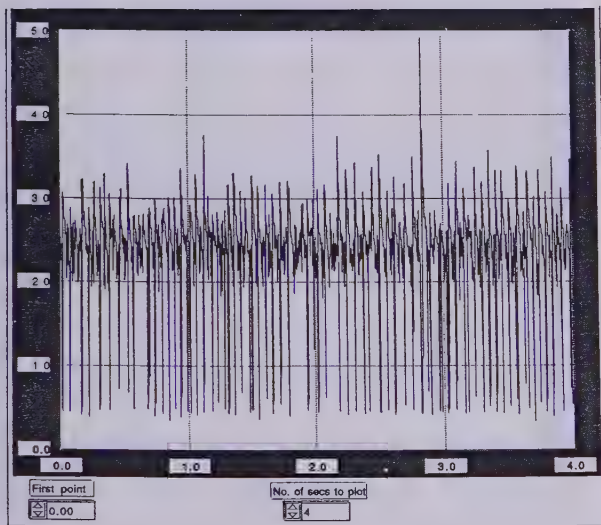




(a) SVI on A36.



(b) PowerWave 450 on A36.



(c) SVI on IPSCO #426507.



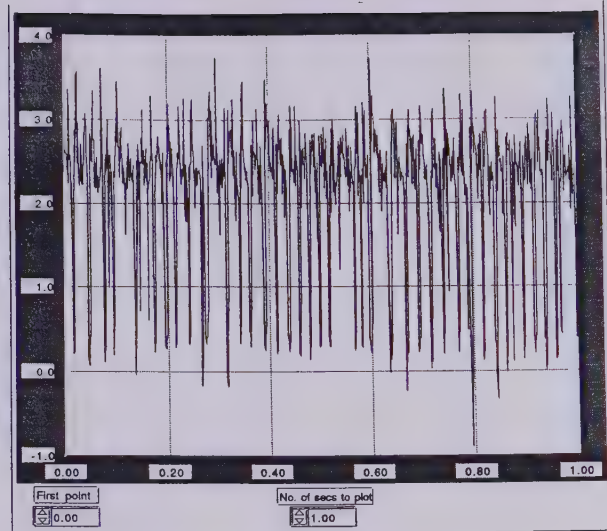
(d) PowerWave 450 on  
IPSCO #426507.

Figure 14: 4 second oscilloscopes (x10 V).

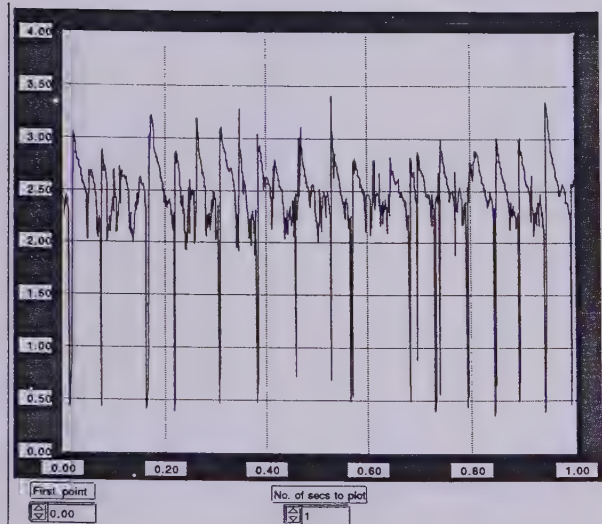




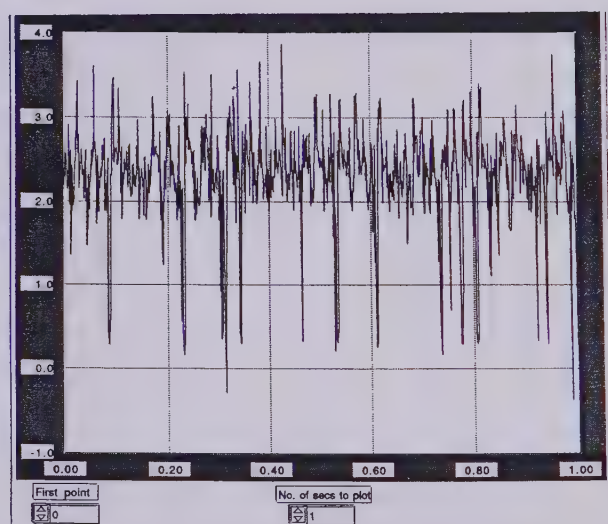
(a) SVI on A36.



(b) PowerWave 450 on A36.



(c) SVI on IPSCO #426507.



(d) PowerWave 450 on IPSCO #426507.

Figure 15: 1.0 second oscillograms (x10 V).





(a) SVI on A36.



(b) PowerWave 450 on A36.



(c) SVI on IPSCO #426507.



(d) PowerWave 450 on IPSCO #426507.

Figure 16: 0.2 second oscillograms (x10 V).



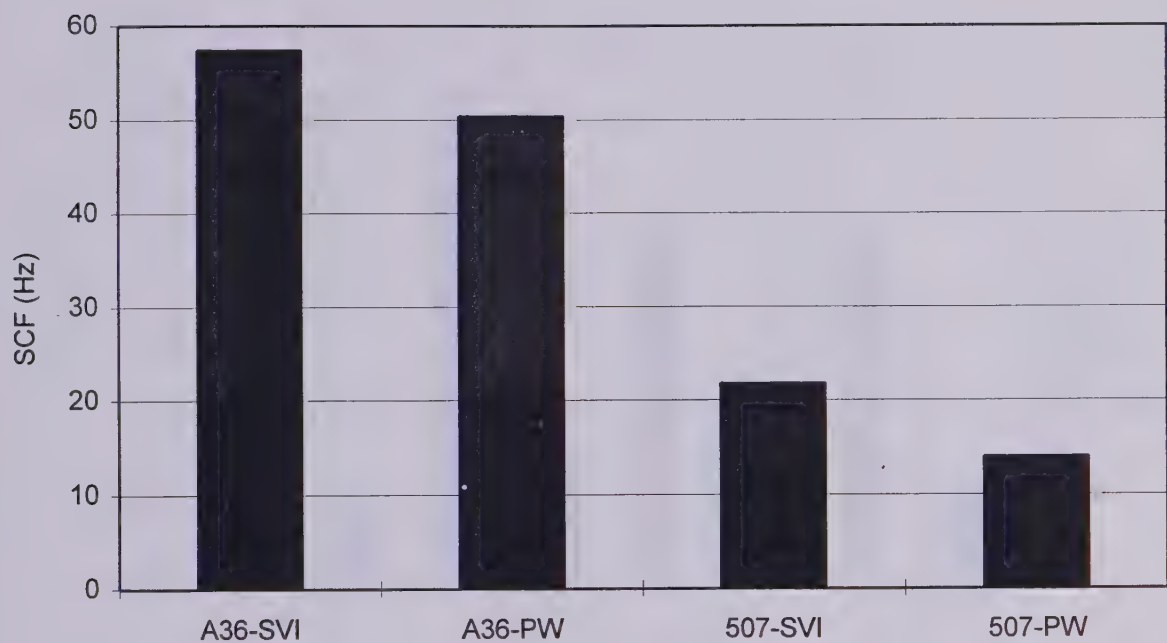


**Figure 17: Short Circuit Frequency (SCF).**



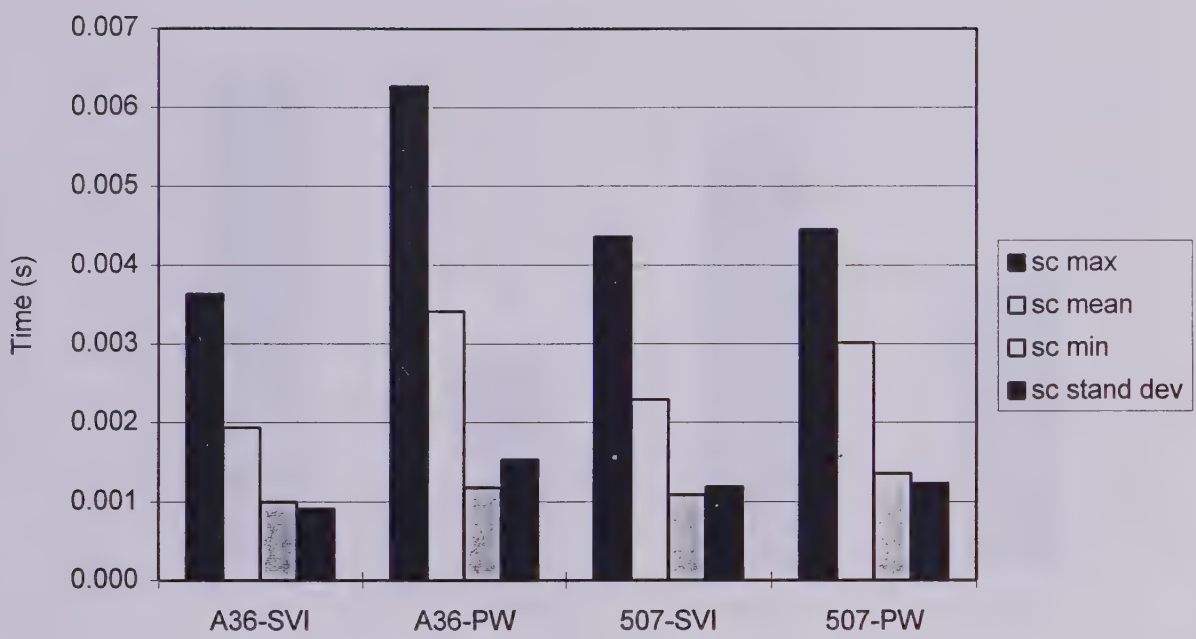


**Figure 18: Short Circuit Duration.**



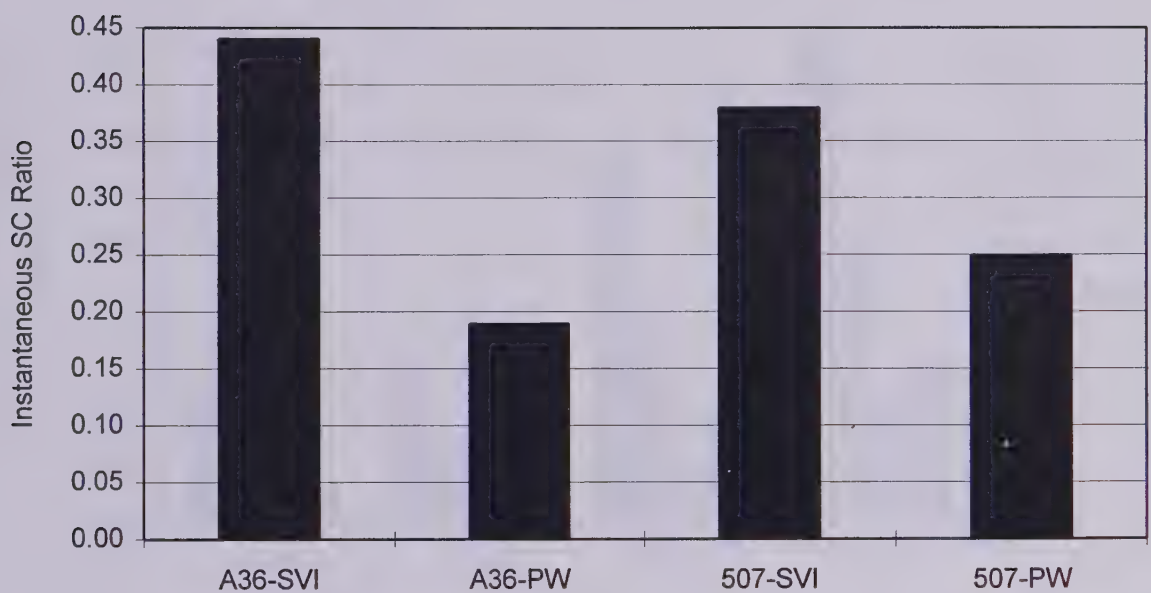


**Figure 19: Instantaneous Short Circuit Ratio.**  
(# of instantaneous short circuits / total # of short circuits)



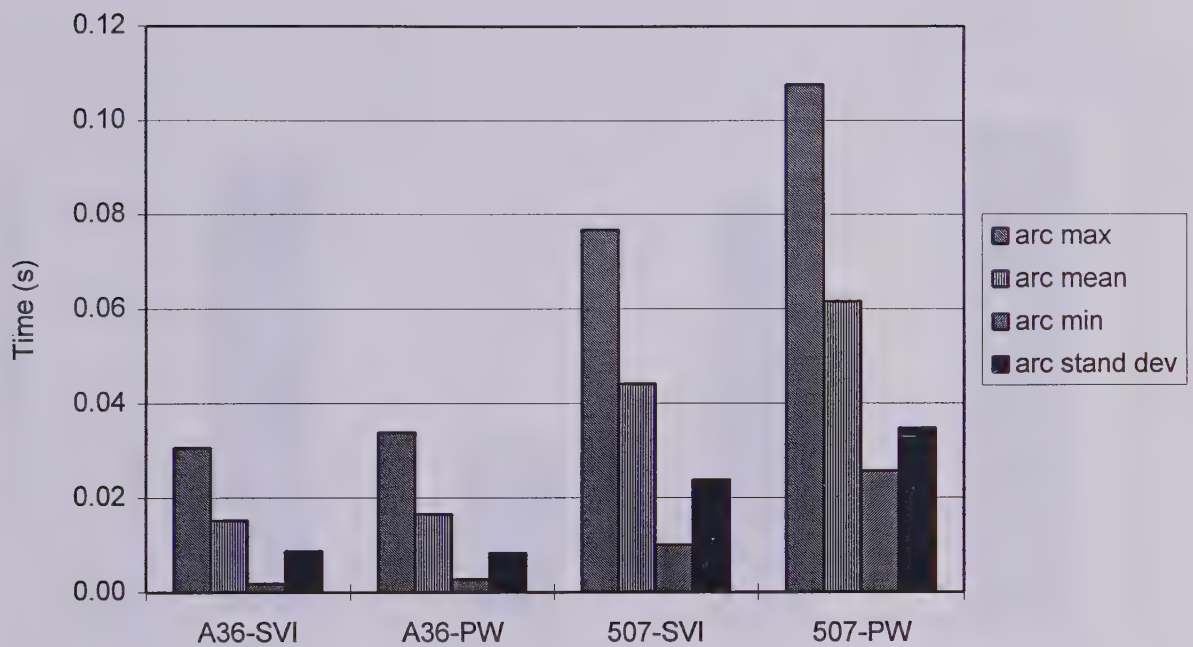


**Figure 20: Arc Duration.**



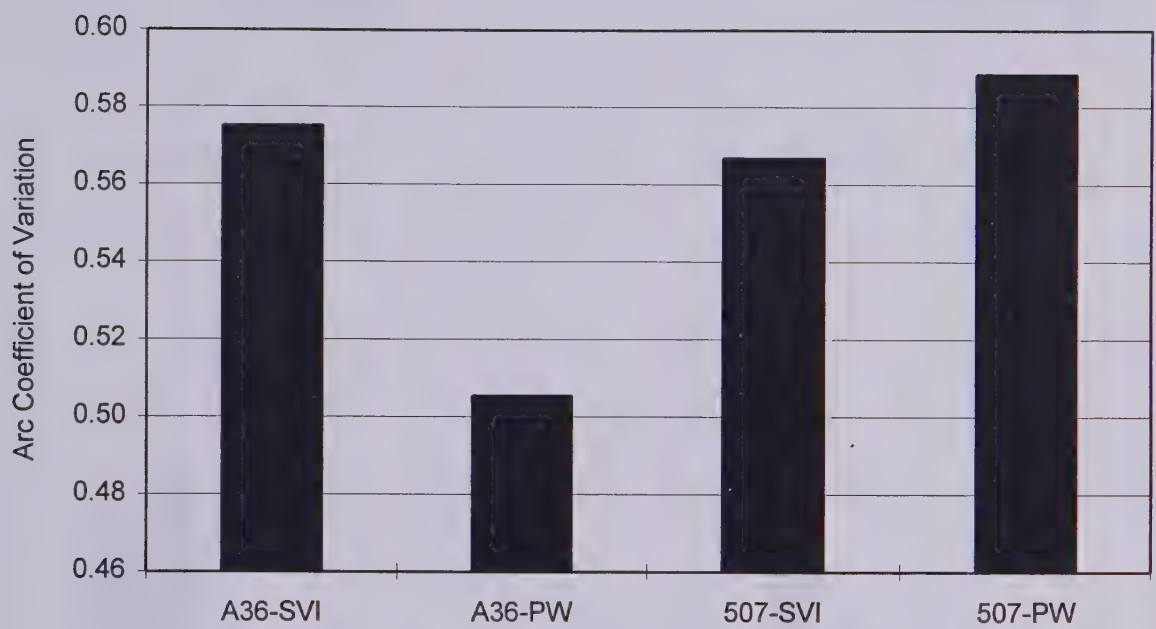
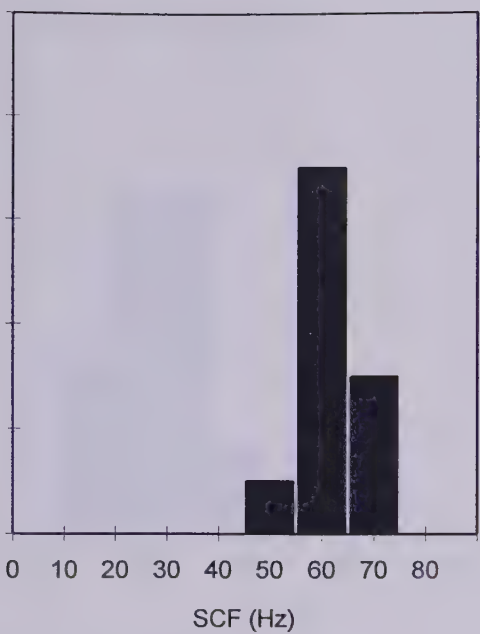


**Figure 21: Arc Coefficient of Variation.**  
(standard deviation of arc duration / mean arc duration)





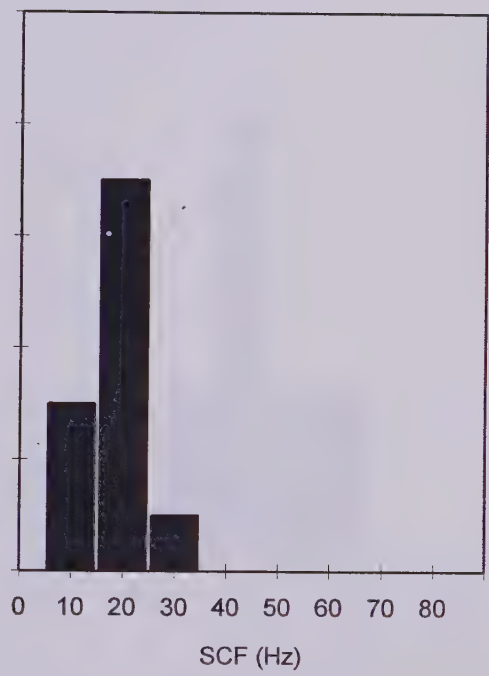
(a) SVI on A36.



(b) PowerWave 450 on A36.



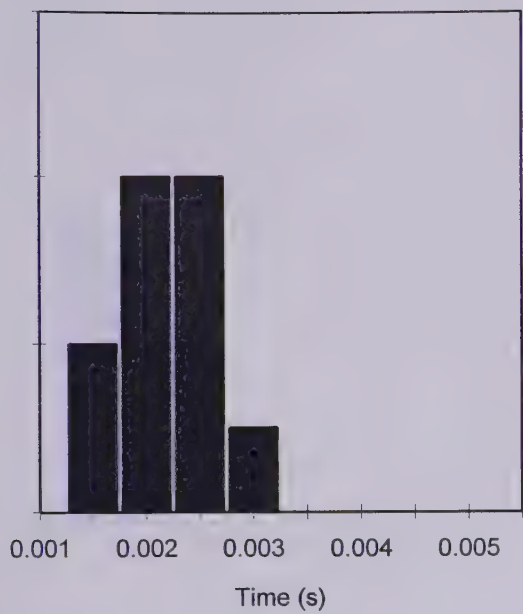
(c) SVI on IPSCO #426507.



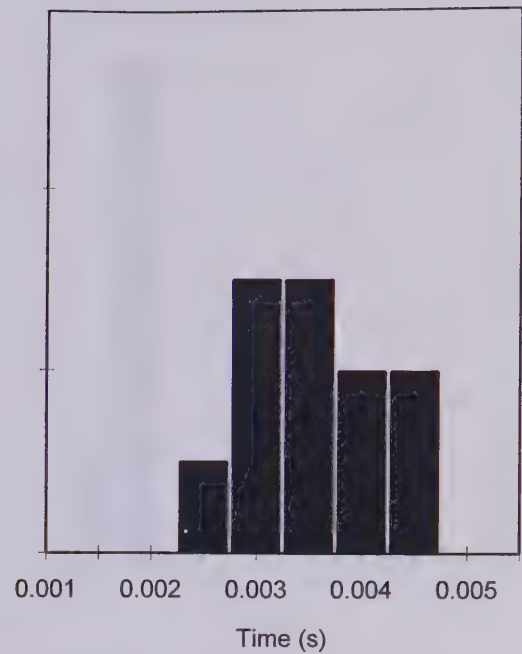
(d) PowerWave 450 on  
IPSCO #426507.

**Figure 22: Histogram of Short Circuit Frequency (SCF).**

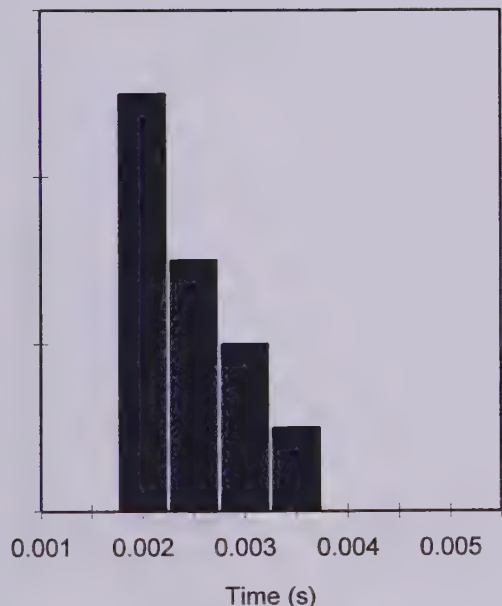




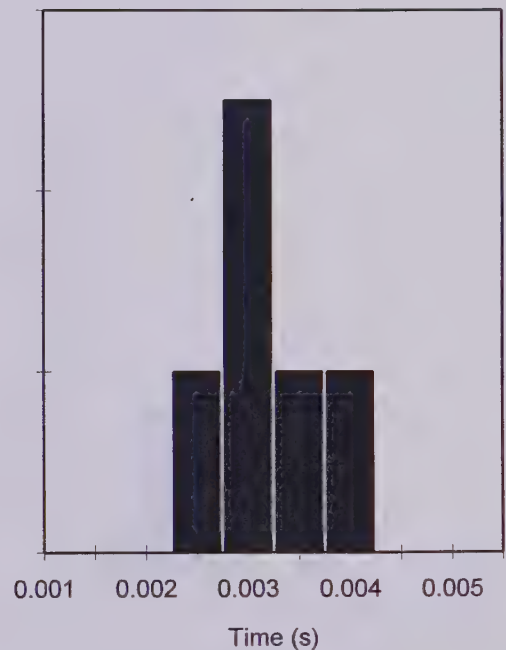
(a) SVI on A36.



(b) PowerWave 450 on A36.



(c) SVI on IPSCO #426507.



(d) PowerWave 450 on IPSCO #426507.

**Figure 23: Short Circuit Duration (Histogram).**

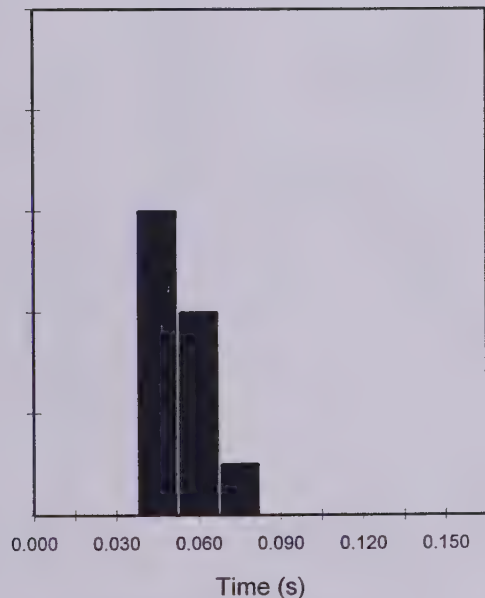




(a) SVI on A36.



(b) PowerWave 450 on A36.



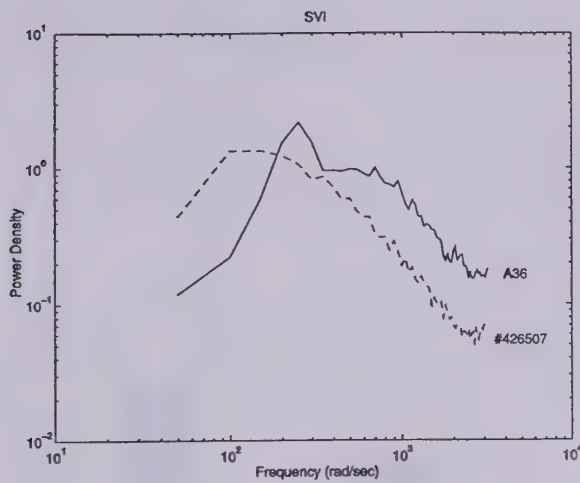
(c) SVI on IPSCO #426507.



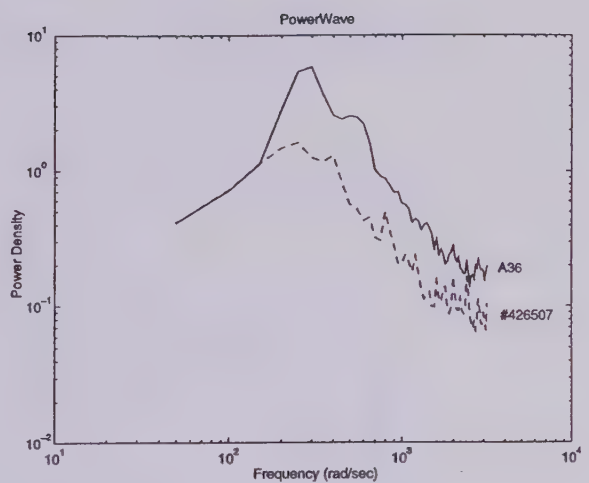
(d) PowerWave 450 on IPSCO #426507.

**Figure 24: Arc Duration (Histogram).**

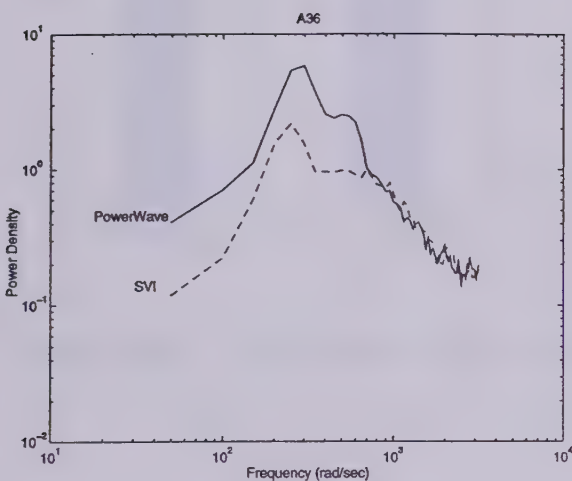




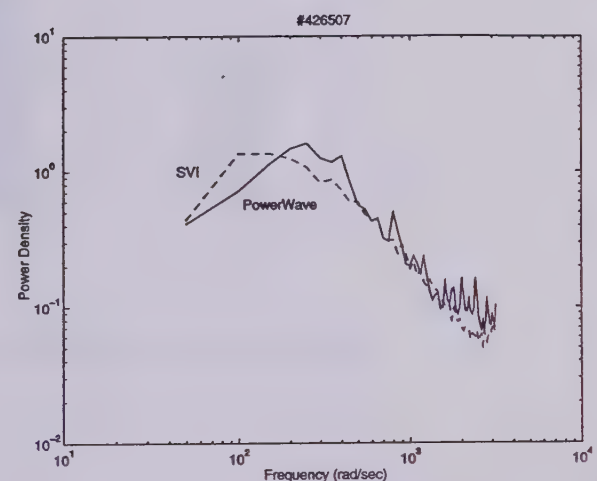
(a) SVI on A36 and IPSCO #426507.



(b) PowerWave 450 on A36 and IPSCO #426507.



(c) SVI and PowerWave 450 on A36.



(d) SVI and PowerWave 450 on on IPSCO #426507.

**Figure 25: Periodograms of GMAW-S.**



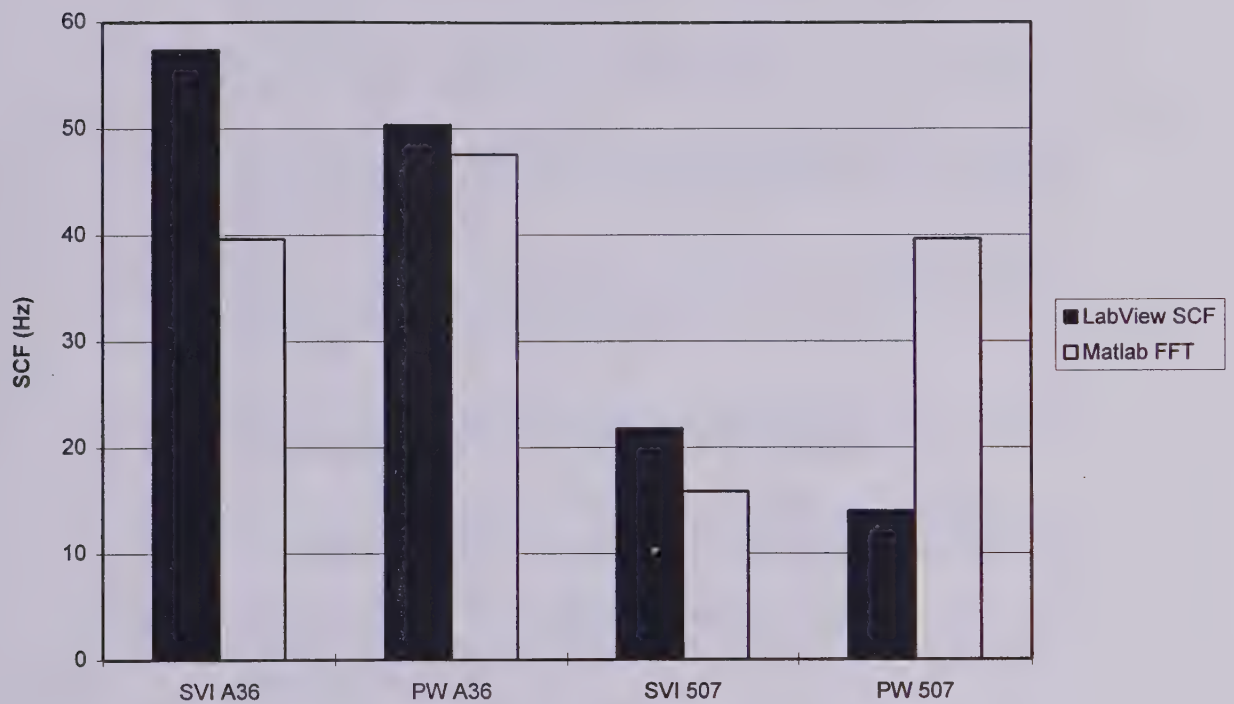


**Figure 26:** Comparison of time and frequency domain SCF.



## 10.0 REFERENCES

- 1) Liu S, Siewert T.A., "**Metal Transfer in Gas Metal Arc Welding: Droplet Rate**," Welding Journal, Vol. 68, No. 2, February 1989, pp 52s-58s
- 2) Patchett B.M., "**MET E 611 - Welding Processes**," Lecture Notes, September 1994
- 3) Lancaster J.F., "**Metallurgy of Welding**," Fifth Edition, Chapman & Hall, 1993, pp 109-113, 121
- 4) Lesnewich A., "**Electrode Activation for Inert-Gas-Shielded Metal-Arc Welding**," The Welding Journal, Vol. 34, No. 12, December 1955, pp 1167-1178
- 5) Michaelson H.B., "**The Work Function of the Elements and its Periodicity**," Journal of Applied Physics, Vol. 48, No. 11, November 1977, pp 4729-4733
- 6) Lancaster J.F. *ed.*, "**The Physics of Arc Welding**," Second Edition, Pergamon Press, 1986, pp 128, 134-136, 169-172
- 7) Patchett B.M., Bicknell A.C., "**Microalloying Effects on GMAW-S Arc Behavior**," IPSCO Project, University of Alberta, 1989
- 8) Li S., Patchett B.M., "**Welding REM-Treated Pipeline Steels with the GMAW-S Process**," AGA Contract PR-152-121, University of Alberta, May 1982
- 9) Naylor K.A., Guile A.E., "**The Effective Drag Width of Short Arc Moving Arcs in Argon**," Journal of Applied Physics, Vol. 18, 1967, pp 1295-1300
- 10) Milner D.R., Apps R.L., "**Introduction to Welding and Brazing**," Pergamon Press, 1968, pp 64-74
- 11) Smith A.A., "**Characterization of the Short Circuiting CO<sub>2</sub> Shielded Arc**," British Welding Journal, Vol. 10, November 1963, pp 571-586
- 12) Waszink J.H., Graat L.H.J., "**Experimental Investigation of the Forces Acting on a Drop of Weld Metal**," Welding Journal, Vol. 62, No. 4, April 1983, pp 108s-116s



- 13) Cooksey C.J., Milner D.R., "**Metal Transfer in Gas-Shielded Arc Welding**," Physics of the Welding Arc - A Symposium, London 1962, Institute of Welding, 1966, pp 123-132
- 14) Glickstein S.S., Yeniscavisch W., "**A Review of Minor Element Effects on the Welding Arc and Weld Penetration**," WRC Bulletin 226, 1976, pp 1-18
- 15) Murthy M.S.P., Loper Jr C.R., "**GMA Weldability Characteristics of Lanthanide-Containing High-Strength Steels, Part 1: Arc and Metal Transfer**," Welding Journal, Vol. 68, No. 2, February 1989, pp 59s-67s
- 16) Ratz G.A., Nippes E.F., Mathew J., Baek W.H., "**The Weldability of Sulphide Shape Controlled Linepipe and HSLA Steels**," Welding Journal, Vol. 63, No. 11, November 1984, pp 333s-338s
- 17) Villafuerte J., Gedeon S.A., "**Counteracting Arc Instability during GMA Welding using Artificial Intelligence Power Supplies**," Welding Institute of Canada Report RC494, May 1995
- 18) Gupta S.R., Gupta P.C., "**Where, Why and How Spatter is Caused in Arc Welding**," Tool & Alloy Steels, Vol. 25, No. 8, August 1991, pp 295-300
- 19) Sasaki H., Akahide K., Tsuboi J., "**CO<sub>2</sub> Short Arc Weldability of Rare Earth Treated Pipeline Steels in Circumferential Welds**," Welding Research Abroad, Vol. 23, No. 11, pp 44-50
- 20) den Ouden G., Xiao Y.H., Hermans M.J.M., "**Oscillation Behavior of the Weld Pool**," Sixth International Conference on the Joining of Materials (JOM-6) [Proc. Conf.], Helsingør, Denmark, April 5-7, 1993, pp 140-149
- 21) Stava E.K., "**A New, Low-Spatter Arc Welding Machine**," Welding Journal, Vol. 72, No. 1, January 1993, pp 25-29
- 22) Nacey T.J., "**Fourth-Generation Inverters Add Artificial Intelligence to the Control of GMA Welding**," Welding Journal, Vol. 72, No. 1, pp 31-34
- 23) Lahnsteiner R., "**Advanced Synergic Inverter Power-Source and Wire-Feed System for GMA-Welding with Integrated Quality Control System**," Welding in the World, Vol. 34, September 1994, pp 205-214



- 24) Lucas W., "Computers in Arc Welding - The Next Industrial Revolution, Part 3: Instrumentation and Process Analysis," Metal Construction, Vol. 17, No. 7, July 1985, pp 431-436
- 25) Pokhodnya I.K. *et al.*, "Metallurgy of Arc Welding, Volume 1: Arc Processes and Electrode Melting," Riecamsky Science Publishing Co., 1991, pp 56-195
- 26) Wang W., Liu S., Jones J.E., "Flux Cored Arc Welding: Arc Signals, Processing and Metal Transfer Characterization," Welding Journal, Vol. 74, No. 11, November 1995, pp 369s-377s
- 27) **Linde Instruction Manual**, Form 11-910-D, February 1977
- 28) **PowerWave 450 - Synergic 7 Instruction Manual**
- 29) Mason D., Lind D., Marchal W., "Statistics, an Introduction," Harcourt Brace Jovanovich, Second Edition, 1988, pp 109-110
- 30) Semeniuk T., "Gas Metal Arc Welding," MET E 611, Welding Processes, Laboratory #3, November 1994, Appendix B
- 31) Beachamp K.G. "Transforms of Engineers - A Guide to Signal Processing," Clarendon Press, 1987, pp 1-47
- 32) The Mathworks Inc., Matlab Version 4.2a **Signal Processing Toolbox Manual**
- 33) Lynn P.A. "An Introduction to the Analysis and Processing of Signals," MacMillan Press, 1973, pp 62-64
- 34) Jenkins G.M., Watts D.G., "Spectral Analysis and its Applications," Holden-Day, 1969, pp 284-286



## **11.0 APPENDICES**



## **APPENDIX A**

### **Chemical Composition of Thyssen K-Nova Wire**



Rudy Tetreau

FROM: R. Wenger  
 CO.:  
 PHONE #:  
 FAX #:

403/448-8350



## THYSSEN SCHWEISSTECHNIK GMBH

Qualitätssicherung  
 Quality Assurance

Thyssen Stahlunion GmbH  
 Thyssen Trade Center  
 H.-G.-Sohl-Str. 1

40235 Düsseldorf

Wilhelmsstraße 2  
 Hamm

FSQW 1 Lo / 16.03.1994

- Werkszeugnis EN 10 204/DIN 50 049-2.2  
 Certificate according to EN 10 204/DIN 50 049-2.2
- Abnahmeprüfzeugnis EN 10 204/DIN 50 049-3.1.B  
 Certificate according to EN 10 204/DIN 50 049-3.1.B
- Certificate of Compliance
- Certified Material Test Report

Bestell-Nr.  
 Your Order No.

1620-7375/5 - CRC / USA

Bestellidatum:  
 Date of Order

10.12.93

Unsere Auftrags-Nr.:  
 Our Order No.

82302762

Prüfgegenstand:  
 Test Object

Drahtelektroden  
 wire electrodes

Nr. Item	Marke Trade Name	Abm. Size mm	Chargen-Nr. Lot/Hazl No.	Norm Specification	Normbezeichnung Classification
1	Thyssen K Nova	0,9	260556	SFA 5.18	ER 70 S-6*)
2					except C = 0,05 %
3					and Si = 0,77 %
4					

Chemische Zusammensetzung des Schweißgusses -drähtes %  
 XXXXXX Filter Metal Analysis

Nr. Item	C	Si	Mn	Cr	Mo	Ni	P	S	Cu**) T1	
1	0,05	0,77	1,50				0,008	0,010	0,13	0,05
2										
3										
4										

We hereby certify that the above product is in compliance with all applicable requirements of the listed specifications

THYSSEN SCHWEISSTECHNIK GMBH

Qualitätssicherung  
 Quality Assurance

Werksachverständiger  
 Internal Surveyor

Bemerkungen:  
 Remarks

\*\*) einschl. Oberflächenverkupferung  
 incl. copper coating



Zeugnis Nr.:  
Certificate No.

039/12

Seite 2 von 2  
Page 2 of 2

Wärmebehandlung:  
Heat Treatment

./.

Schutzgas/shielding gas: CO<sub>2</sub>

Mechanische Gütekriterien des reinen Schweißgutes nach DIN  
Mechanical Properties of the All-Weld Metal according to DIN

Zugversuch  
Tensile Test

Prüftemperatur:  
Test Temperature 20 °C

Nr. Item	0,2 %-Dehngrenze Yield Strength at 0,2 % Oberspannung R <sub>p</sub> (N/mm <sup>2</sup> )	Streckgrenze Yield Strength R <sub>eH</sub> (N/mm <sup>2</sup> )	Zugfestigkeit Tensile Strength R <sub>m</sub> (N/mm <sup>2</sup> )	Dehnung Elongation Zin A <sub>z</sub> (%)	Einschnürung Reduction of Area Z (%)
1	460	474	545	33,8	72
2					
3					
4					

Kerbschlagbiegeversuch  
Impact Test

Probenform:  
Shape of Specimen CVN

Einheit:  
Dimension Joule

Prüftemperatur:  
Test Temperature minus 29°C

Nr. Item	Kerbschlagarbeit Impact energy							
1	86/66/48/54/68							
2								
3								
4								

Herstellung und Kontrolle der Schweißzusätze erfolgten nach  
The a.m. welding filler metals have been manufactured and supervised according to

Soundness test / Röntgenprüfung gemäß SFA 5.18

Bemerkungen:  
Remarks Ergebnis: keine erkennbaren Fehler - Anforderung nach SFA 5.18 erfüllt.  
The radiographic test results meet the requirements of SFA 5.18.

THYSSEN SCHWEISSTECHNIK GMBH

Qualitätssicherung  
Quality Assurance

Werksseidivierständiger  
Internal Surveyor



## **APPENDIX B**

### **Matlab & Unix Commands for Spectral Analysis**



## Matlab Commands

LabVIEW data acquisition files should be in “tab delimited” configuration, i.e., a row vector.

To load LabVIEW files into a Unix (Matlab) directory, first find a network computer with a floppy disk drive and open Matlab. Then enter:

```
>> load a:filename; w=filename; w=w(:); plot(w)
```

The following commands will generate the spectral analysis plots of Power Density vs. Frequency provided the following files exist in the users directory:

- 1) spectral.m
- 2) ssp.m

Be careful the code does not get modified in the file transfer (happened to me).

*Italics* indicate Matlab response and “>>” indicates typed commands. “Help” is also available.

```
>> diary on  
>> dir  
>> load w  
>> load x  
>> load y  
>> load z  
>> [f,m]=spectral(w,0.001,5,1,'hanning');  
*****
```

*This usage of inverf(X) is obsolete and will be eliminated in future versions. Please use erfinv(X) instead.*

The preceding error message may indicate one of the above files (spectral.m or ssp.m) may require modification of the computer code in the future. This line is at the very end of the code. It is expected that replacing “inverf(X)” by “erfinv(X)” would eliminate this error message. In this application the two subroutines are equivalent and there would be no change in the results.

The parameter “5” can be varied to control the amount of smoothing that occurs. This parameter is related to the data segmenting. Increasing this value gives greater smoothing but means that fewer frequency points are produced, i.e., a



trade-off exists. Note that a value of “5” represents fairly strong smoothing. 0.001 is the sampling frequency.

```
>> [f1,m1]=spectral(x,0.001,5,1,'hanning');
>> [f2,m2]=spectral(y,0.001,5,1,'hanning');
>> [f3,m3]=spectral(z,0.001,5,1,'hanning');

>> loglog(f,m,f1,m1);title('A36');ylabel('Power Density (dB)');xlabel('Frequency
(rad/sec)');
>> gtext('PowerWave');gtext('SVI');
>> loglog(f,m,'-',f1,m1,'--');title('A36');ylabel('Power Density
(dB)');xlabel('Frequency (rad/sec)');
>> gtext('PowerWave');gtext('SVI');
>> print a36
>> dir
```

```
>> more on
>> more off
```

The “more ” commands stop the screen from scrolling.

```
>> plot(f,m,'-',f1,m1,'--');title('A36');ylabel('Power Density
(dB)');xlabel('Frequency (rad/sec)');
>> gtext('PowerWave');gtext('SVI');
>> a=max(m);disp(a);
      5.8137
>> b=max(m1);disp(b);
      2.1821
>> c=max(m2);disp(c);
      1.5998
>> d=max(m3);disp(d);
      1.3470
>> diary on
```

To find the frequency corresponding to the maximum power density:

```
>> mmax=max(m)
      mmax =
      5.8137
>> k=find(m==mmax)
      k =
      6
```



```

>> freqmax=f(k)
    freqmax =
    299.1993
>> mmax=max(m1)
    mmax =
    2.1821
>> k=find(m1==mmax)
    k =
    5
>> freqmax=f(k)
    freqmax =
    249.3328
>> mmax=max(m2)
    mmax =
    1.5998
>> k=find(m2==mmax)
    k =
    5
>> freqmax=f(k)
    freqmax =
    249.3328
>> mmax=max(m3)
    mmax =
    1.3470
>> k=find(m3==mmax)
    k =
    2
>> freqmax=f(k)
    freqmax =
    99.7331
>> diary off

```

Other useful commands include:

- 1) To set graph axes:  
([xmin xmax ymin ymax])
- 2) To freeze scaling:  
axis(axis)
- 3) To hold current plot settings:  
hold on, hold off, hold (toggles between hold on and hold off).



## Aixterm Window

To print from Matlab:

- 1) Open another aixterm window or exit Matlab.
- 2) Type “ls” to look at directory.
- 3) Type: prnt -ps *filename.ps*



## **APPENDIX C**

### **FFT Frequency Conversion**



## FFT Frequency Conversion

LabVIEW was used for data acquisition and Matlab for FFT spectral analysis. Matlab generates frequency in units of radians per second (rad/sec) whereas LabVIEW frequency is given in cycles per second (Hz). To convert rad/sec to Hz:

$$\omega = 2\pi f \text{ and therefore } f = \omega/2\pi$$

where:  $\omega$  = frequency (rad/sec)  
 $f$  = frequency (cycles/sec)  
 $t$  = time (sec)

Example #1: Say the peak FFT spectral analysis frequency occurs at  $\omega = 240$  rad/sec.

$$\text{then } f = (240 \text{ rad/sec})/ 2\pi = 38.2 \text{ Hz} = \text{SCF}$$

Example #2: To find the time period of one cycle, if the peak FFT spectral analysis frequency occurs at  $\omega = 240$  rad/sec:

$$\omega = 2\pi f, \text{ and since } f=1/t$$

$$t = 2\pi/\omega = 2\pi/240 \text{ rad/sec} = 0.026 \text{ sec}$$

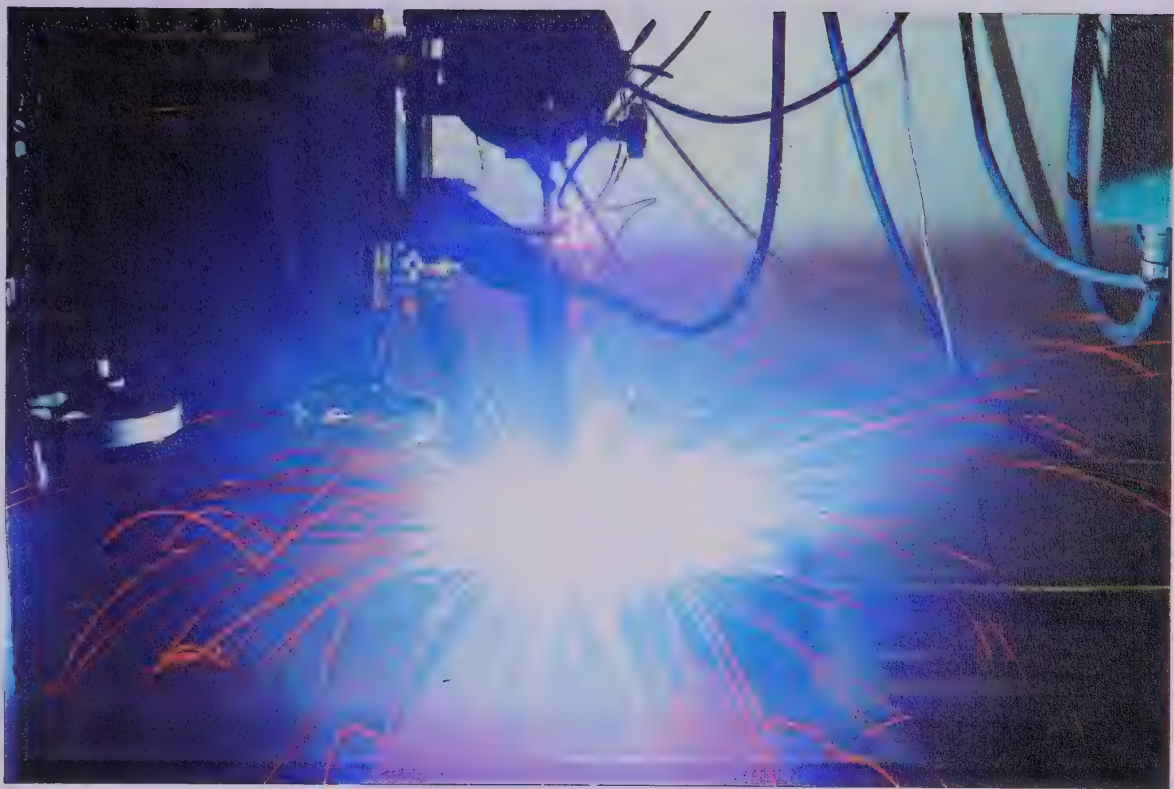
and 0.026 sec is also equal to 1/SCF.



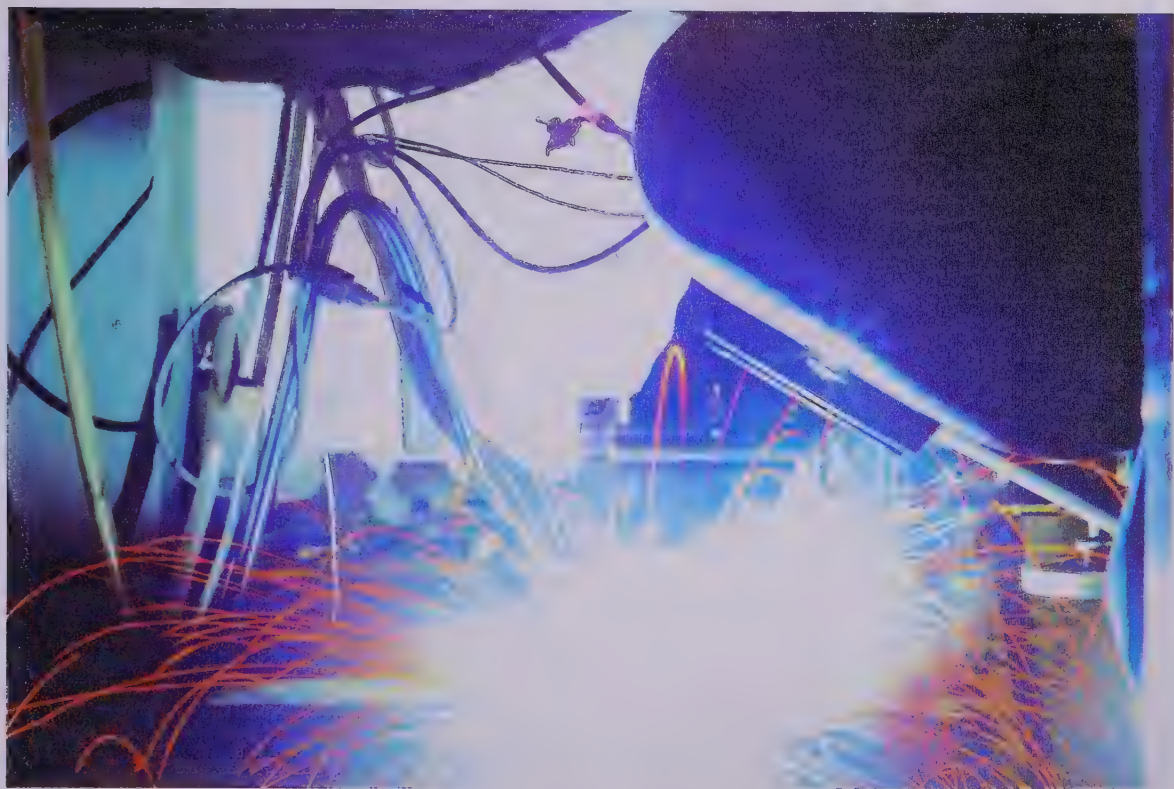
## **APPENDIX D**

### **Initial Spatter Spark Trail Photographs**





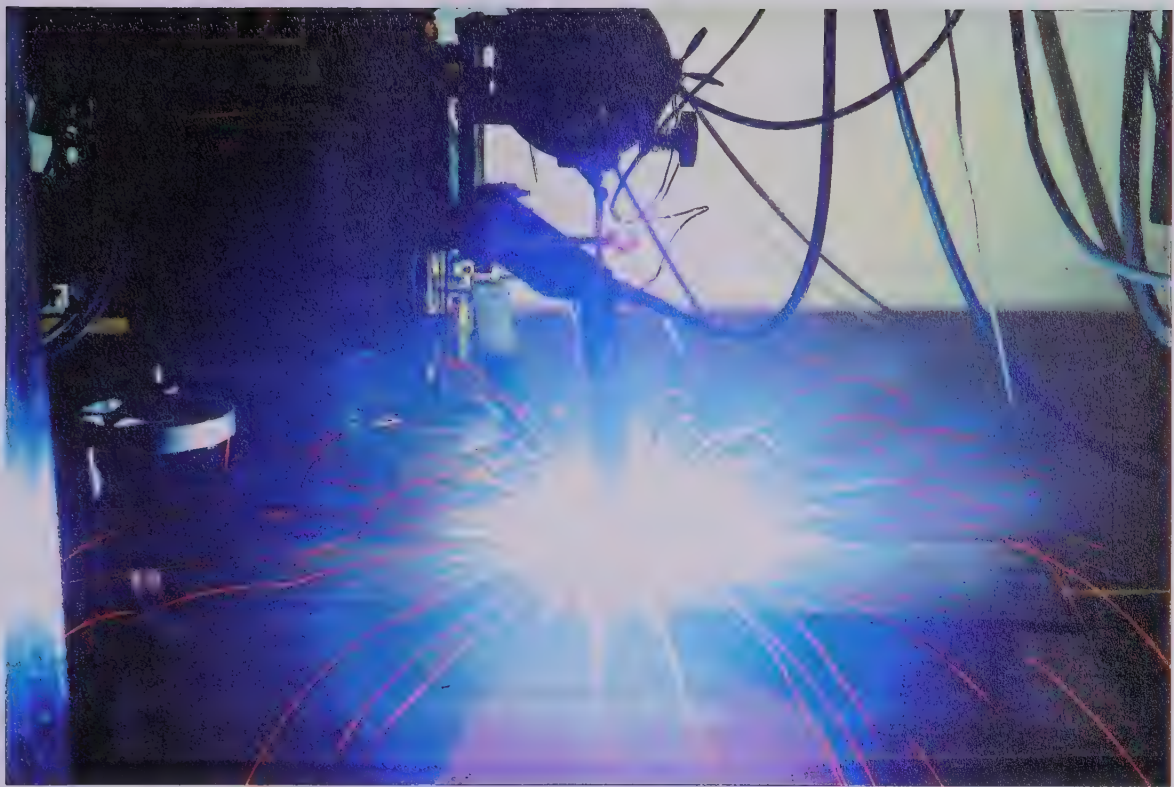
(a) SVI on A36.



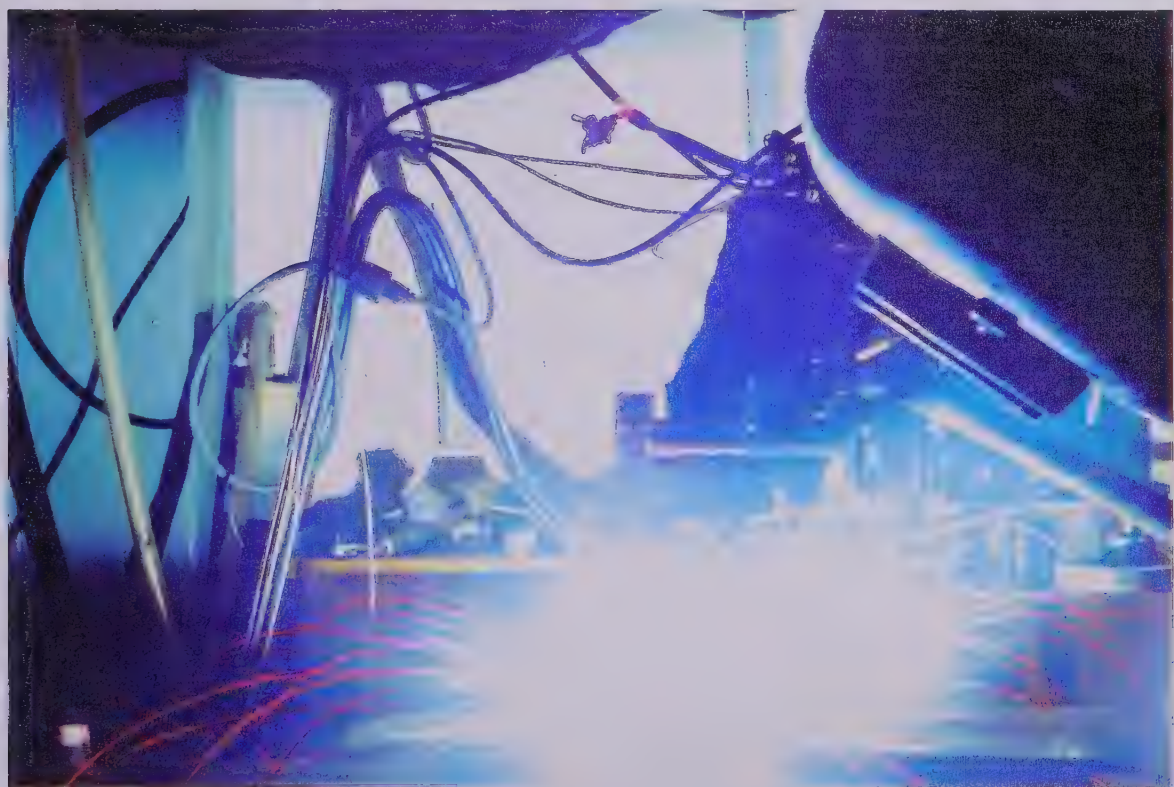
(b) PowerWave 450 on A36.

**Figure D1: Spatter spark trail photographs.**





(c) SVI on #426507.



(d) PowerWave 450 on #426507.

**Figure D1:** Spatter spark trail photographs.



## **APPENDIX E**

### **Parametric Spectral Analysis of Linde SVI on A36**



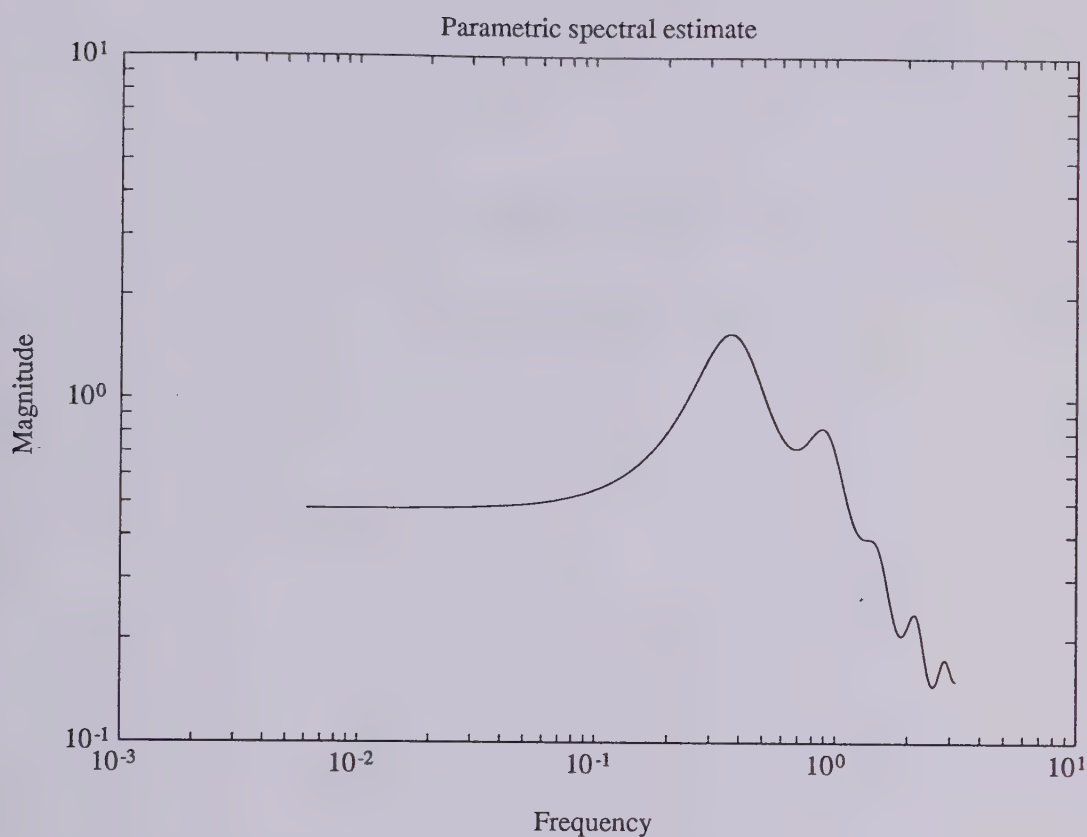


**Figure E1: Parametric Spectral Analysis of Linde SVI on A36.**



## **APPENDIX F**

### **Research Agreement**



## **RESEARCH GRANT AGREEMENT**

AN AGREEMENT MADE the 28th day of September, 1995

BETWEEN:

**NOVA GAS TRANSMISSION LTD.**  
PO Box 2535, Station M  
Calgary, Alberta  
T2P 2N6

-and-

**LINCOLN ELECTRIC COMPANY OF CANADA LTD.**  
#6 - 5925 12th Street S.E.  
Calgary, Alberta  
T2H 2M3

(referred to collectively as "Sponsors")

- and -

**THE GOVERNORS OF THE UNIVERSITY OF  
ALBERTA,**  
a corporation under the Universities Act, R.S.A. 1980, c.  
U-5, Edmonton, Alberta T6G 2J9  
(referred to as the "University")

WHEREAS Sponsors wishes to support a research project entitled Arc Instability in Mechanized Gas Metal Arc Welding (the "Research") as described in Schedule "A", and share in the results of the Research for mutual benefit,

AND WHEREAS Lincoln agrees to provide equipment Lincoln Power Wave 450, on loan only, and associated software

AND WHEREAS NOVA agrees to pay \$13562 and supply materials upon the signing of this Agreement in accordance with the budget attached as Schedule "B".

The University and Sponsors hereby agree as follows:

### **1. PERIOD OF AGREEMENT**

This Agreement shall be effective from October 1, 1995 to May 31, 1996 unless otherwise extended, renewed, or amended by mutual written consent.



## **2. PERSONNEL**

The University agrees that the Research shall be undertaken under the direction of the Project Leader, Dr. BM Patchett of the Department of Mining, Metallurgical and Petroleum Engineering. Mr. Taras Semeniuk would be the principal researcher. Mr. Clark Bicknell would provide technical support. The Project Leader shall have responsibility for the conduct of the research project.

## **3. SHARING OF RESULTS**

Sponsors and the University will be provided with all results and reports of the Research within 90 days from May 31, 1996. Sponsors will be acknowledged in any anticipated presentations and papers associated with this data. The University shall provide to Sponsors a royalty free non-exclusive right to use project results for internal commercial research and development purposes for their products. Nothing in this Agreement can be construed as a license to use University or Joint Intellectual Property for any commercial purpose. However, the University of Alberta will grant sponsors right to negotiate an exclusive license.

## **4. INTELLECTUAL PROPERTY**

**4.1** Intellectual property ("Intellectual Property") includes, but is not limited to, substances, processes, formulations, technical information, reports, photographs, drawings, plans, specifications, models, prototypes, inventions, patterns, samples, designs, or know-how, whether patentable or not.

**4.2** Any Intellectual Property solely invented by the University ("University Intellectual Property") arising from the Research shall be owned by the Project Leader and/or the University in accordance with the policies of the University.

**4.3** Any Intellectual Property jointly invented by the University and Sponsors and/or other collaborators shall be owned jointly by the inventing parties ("Joint Intellectual Property").

**4.4** Any Intellectual Property solely invented by Sponsors arising from the Research shall be owned by Sponsors ("Sponsors Intellectual Property"). Any and all waveforms and programs developed for the Lincoln Invertec PowerWave are and will remain the exclusive property of Lincoln Electric. Sponsors and the University agree that the Lincoln single user software license agreement M17744 is an accepted and integral part of this research grant agreement.

## **5. PUBLICATION RIGHTS**

Sponsors shall be furnished with copies of any proposed publication relating to this Agreement at least sixty (60) days in advance of presentation or publication. If requested, University of Alberta will publish jointly with Lincoln Electric Company of Canada Ltd. and/or Nova Gas Transmission Ltd. should the results warrant publication. If requested, publication or presentation can be delayed 6-9 months for Intellectual Property protection process.

## **6. EQUIPMENT**

Equipment purchased for use in the Research shall be the property of the purchasing party unless specified otherwise.



## **7. WARRANTY**

The University agrees to carry out the Research in accordance with high scientific and professional standards but does not promise success in achieving any desired result. The University gives no warranty of fitness for a particular purpose, or any other warranty, express or implied, on the results of the Research. The University shall not be liable for any direct, consequential, or any other damage suffered by Sponsors or others resulting from the use of the Research results or any invention, technology or product produced in the course of or using the results of the Research.

## **8. TERMINATION**

**8.1** This Agreement may be terminated by any party by giving sixty (60) days written notice to the other parties. In the event of termination, the University and Sponsors shall take all necessary steps to effect the orderly termination of the Research, including any final reporting required.

**8.2** The provisions of Articles 4, 6, 7, 8, 9, and 10 shall survive termination of this Agreement.

## **9. INDEMNIFICATION**

**9.1** Sponsors agrees to hold harmless, indemnify and defend the University from all liabilities, demands, damages, expenses and losses arising out of the use by Sponsors or by any party acting on behalf of or under authorization from Sponsors of University technical development or out of any use, sale or other disposition by Sponsors, or by any party acting on behalf of or under authorization from Sponsors of products made by use of the University technical developments.

**9.2** The University agrees to hold harmless, indemnify and defend Sponsors from all liabilities, demands, damages, expenses and losses arising out of the use by the University or by any party acting on behalf of or under authorization from the University of Sponsor's technical development or out of any use, sale or other disposition by the University, or by any party acting on behalf of or under authorization from the University of products made by use of Sponsors' technical developments.

## **10. AMENDMENT**

No Amendment or variation to this Agreement shall operate to change or vary the terms, obligations, or conditions hereof except upon mutual agreement by all parties signed by authorized representatives of each party.



## **11. NOTICES**

All notices, requests, directions, or other communications required or permitted herein shall be in writing and shall be delivered to the parties hereto respectively as follows:

### **UNIVERSITY:**

Industry Liaison Office

1-3 University Hall  
University of Alberta  
Edmonton, Alberta T6G 2J9  
Attn: Sharlene Coss, Contracts Manager  
ph. (403) 492-5670  
Fax (403) 492-7876

### **SPONSORS:**

Nova Gas Transmission Ltd.  
PO Box 2535, Station M  
Calgary, Alberta  
T2P 2N6  
Attn: David Dorling  
ph. (403) 290-6647  
Fax (403) 290-7178

Lincoln Electric Company of Canada Ltd.  
#6 - 5925 12th Street S.E.  
Calgary, Alberta  
T2H 2M3  
Attn: Rob Armour  
ph. (403) 253-9600  
Fax (403) 252-5863

In order for any notices, requests, directions, or other communications to be effective, they shall be delivered in person; or, sent by registered mail, telegram, telex or facsimile addressed to the party for whom it is intended at the above mentioned address and shall be deemed to have been received, if sent by registered mail, when the postal receipt is acknowledged by the other party; if sent by telegram, when transmitted by the carrier; and, if sent by telex or facsimile, when transmitted. The address of either party may be changed by notice in the manner set out in this provision.

## **12. GOVERNING LAW**

This Agreement shall be governed by and interpreted in accordance with the laws of the Province of Alberta and the parties hereby expressly attorn to the jurisdiction of the courts of Alberta for enforcement thereof.

**IN WITNESS WHEREOF**, the duly authorized officers of the parties have executed this Agreement on the date first written above.

Per: University of Alberta

Per: Nova

Per: Lincoln

---

Project Leader

David Dorling

---

Rob Armour

---

Principal Investigator

---

Mike Brooks

---

Department Chairman

---

Faculty Dean

---

Industry Liaison Office



## SCHEDULE "A"

This is Schedule "A" attached to and forming part of the Agreement dated as of the effective date and entered into between the University and the Contractor.

In steelmaking, Calcium is added to modern pipeline steels to minimize sulphur levels and modify inclusion morphology. Unfortunately, Ca based oxysulphide inclusions may detrimentally affect the stability of the welding arc causing plasma flaring which may induce flaws in the weld-bead, e.g. step-like defects and lack of fusion.

The proposed research work will attempt to control arc stability in short circuit gas-metal arc welding (GMAW-S) using a programmable power supply. In simple terms, the equipment would be used to instantaneously decrease arc voltage when the arc flare duration exceeds a pre-set time. It is thought that this action would over-ride Calcium (and Cerium) inclusion induced arc flaring, thus promoting a more regular short circuit metal transfer event.

If successful, the benefit would be an improvement in weld quality, and potentially, a decrease in pipeline construction costs.



## SCHEDULE "B"

This is Schedule "B" attached to and forming part of the Agreement dated as of the effective date and entered into between the University and the Contractors.

### Estimated Costs:

#### A. Literature Survey

T. Semeniuk - 1 month @ \$400	\$400	\$400
-------------------------------	-------	-------

#### B. Materials & Supplies

gases	\$400	
high speed video	\$400	
pipe & consumables - Nova supply	N/C	
Powerwave 450 & software - Lincoln supply	N/C	\$800

#### C. Experimentation

T. Semeniuk - 4 months @ \$400	\$1600	
C. Bicknell - 2 months @ \$3202	\$6404	
benefits @ \$607	\$1214	\$9218

#### D. Reporting

T. Semeniuk - 3 months @ \$400	\$1200	
B. Patchett - 1/4 day @ \$700/day	\$175	\$1375

#### E. University Overhead - 15%

\$1769

**Grand Total** **\$13562.00**









ot of Mining, Metallurgical  
nd Petroleum Engineering  
University of Alberta  
Edmonton, Alberta  
Canada T6G 2G6

